CFD simulation of multiphase twin screw pump

van Beijnum, M.

Award date:
2007

CFD simulation of multiphase twin screw pump

M. van Beijnum
Report number: WPC 2007.08

Committee:
Prof. dr. ir. J.J.H. Brouwers (chairman)
Dr. B.P.M. van Esch (supervisor)
Dr. J.G.M. Kuerten
Dr. ir. C.C.M. Rindt
Dr. ir. O.J. Teerling

Technische Universiteit Eindhoven
Department of Mechanical Engineering
Division TFE, Section Process Technology

Eindhoven, August 2007

Abstract

Multiphase pumping in the oil and gas industry is the ability to boost pressure without separating the liquid and the gas phases. This gives opportunities to process the different phases centrally when using multiple well sites, or processing on land for an offshore well. No separation of the phases and only one pipeline have to be used. For optimal performance of a twin screw pump a small liquid fraction is necessary to seal the internal clearances of a twin screw pump. 100 percent gas void fractions can be pumped for a short period of time when arrangements are made to recirculate fluid, to seal the clearances. This makes the internal design of a twin screw pump an engineering challenge. To gain more insight of the flow in a twin screw pump a CFD model can be used.

The goal of this graduation report is to predict the leakage flow rate in a twin screw pump with a three-dimensional model of the pump and a commercial CFD package. This goal can be divided in three parts. The leakage flow rate first for non-rotating screws and single-phase flow, secondly for rotating screws and single-phase flow, and finally considering multiphase flow with rotating screws. In this report the first part is considered, and recommendations are given for the other parts.

The leakage flow rate is simplified in two different cases. The first case is flow through an annulus with inner rotating cylinder, this represents the flow between the screw and housing (liner) of a twin screw pump. The second case is flow through a straight-through labyrinth seal. The screw thread viewed in axial direction is similar to a labyrinth seal. Recirculation and throttling of fluid in the screw cavities can be expected. For these two cases the performance of the turbulence model is evaluated and coupled to requirements for the dimensionless wall distance in the first cell near the wall.
To simulate the flow in a twin screw pump the flow domain has to be meshed, the mesh must have a limited number of cells to perform calculations with normal PC requirements in a reasonable amount of time. The number of cells in the clearance between the tips of the screw and the liner is estimated. The number of cells with an unstructured tetrahedral mesh is too large to perform CFD simulations. Structured hexahedral cells can be used, however these cells have to be elongated in axial and tangential direction to reduce the number of cells. A structured grid with hexahedral cells is created by layering cross-sections perpendicular to the axial direction. The cells on a cross-section are placed along gradient lines of the Laplace problem solved for this cross-section. The Laplace problem is solved, for an unstructured triangular mesh of the cross-section, with a mesh generator and solver of a commercial CFD package. Gradient lines never cross each other, so a robust two-dimensional grid is created. For the next cross-section, a small displacement in axial direction, the screws are rotated slightly and the Laplace problem is solved again. Merging the cross-sections gives a three-dimensional grid

of the screws of a twin screw pump. The quality of this three-dimensional grid is examined. The low screw pitch gives a relatively large tangential displacement compared to the axial displacement, resulting in highly skewed cells. This reduces the applicability of this grid for turbulent flows. Elongating the screws in axial direction (higher pitch) gives a better quality grid, however the original geometry is lost.

The leakage flow through a twin screw pump has two paths, first, leakage through the clearance between the screw and the liner, and secondly between the screws itself. The leakage flow through the twin screw pump is simulated for a differential pressure of up to 10 kPa per screw thread (seal) on the three-dimensional grid. For higher differential pressures the simulation does non converge. The simulated leakage flow rate in the clearance between screw and liner is approximately the same as the analytic laminar leakage flow rate through a stationary annulus. The relation between differential pressure and leakage flow rate is determined for low axial Reynolds numbers, and for higher axial Reynolds numbers using an elongated grid in axial direction.

The static numerical simulation of the flow in a twin screw pump show realistic flow features. The differential pressure per screw thread has to be increased to simulate real pump performance. The numerical model is created with the ability to add a dynamic mesh, this to simulate the rotation of the screws. Also multiphase models can be added to predict leakage flow characteristics with liquid-gas mixtures. For these extensions to the current model recommendations are given.

Nomenclature

Symbol	Description	[Unit]
a	edge length of cell	$[m]$
A_{cl}	projected area of clearance between screw and liner perpendicular to the axial direction	$[m^2]$
A_{liner}	area of two joined circles	$[m^2]$
A_{screw}	area of screw cross-section	$[m^2]$
D	outer diameter screw	$[m]$
d_h	hydraulic diameter	$[m]$
e	elongation of grid	[-]
f_{AR}	aspect ratio of cell edges	[-]
h	center distance screws	$[m]$
h_1	height of screw cavity	$[m]$
GVF	gas void fraction	[-]
L	length	$[m]$
L	screw thickness	$[m]$
$\dot{m}$	mass flow rate	$[kg/s]$
Ma	Mach number	[-]
N	rotation speed	$[rpm]$
n_{ax}	number of axial cells	[-]
n_{cell}	number of cells in radial direction	[-]
n_{tan}	number of tangential cells	[-]
n_{rev}	number of screw threads (revolutions)	[-]
n_{str}	number of structured cells	[-]
n_{unstr}	number of unstructured cells	[-]
R	outer radius of screw	$[m]$
r_i	inner radius of screw	$[m]$
R_{liner}	radius of liner	$[m]$
Re	axial Reynolds number	[-]
Re_ω	tangential Reynolds number	[-]
s	clearance between screw and liner	$[m]$
p	absolute pressure	$[Pa]$
Δp	pressure difference	$[Pa]$
q	grow rate	[-]
r	pitch of one screw thread	$[m/rev]$
Q_cl	leakage flow rate in clearance between screw and liner	$[m^3/s]$

Symbol	Description	[Unit]
Q_l	leakage flow rate of pump	$[m^3/s]$
Q_r	realized flow rate of pump	$[m^3/s]$
Q_t	theoretical flow rate of pump	$[m^3/s]$
u_τ	friction velocity	$[m/s]$
v	fluid velocity	$[m/s]$
$\langle v_{ax} \rangle$	mean axial velocity	$[m/s]$
V_{cl}	volume of clearance between screw and liner	$[m^3]$
V_D	screw displacement volume per revolution	$[m^3/rev]$
V_{hex}	volume of hexahedral cell	$[m^3]$
V_{tet}	volume of tetrahedral cell	$[m^3]$
y^+	dimensionless wall distance	[-]

Greek symbols

Symbol	Description	[Unit]
θ	angle	$[rad]$
λ	resistance coefficient	[-]
μ	dynamic viscosity	$[kg/(ms)]$
ν	kinematic viscosity	$[m^2/s]$
τ	shear tensor	$[N/m^2]$
τ_w	wall shear stress	$[N/m^2]$
Φ	potential	[-]
ρ	density	$[kg/m^3]$
ω	angular velocity of the screw	$[rad/s]$

Contents

Chapter 1

Introduction

Screw pumps are a special type of rotary positive displacement pump in which the flow through the pumping element is axial. The liquid is carried between screw threads on one or more screws and is displaced axially as the screws rotate and intermesh (see figure 1.1). In all other rotary pumps the liquid is forced circumferentially, thus giving the screw pump its unique axial flow pattern and low internal velocities a number of advantages in many applications where liquid agitation or churning is not desired. Another property for a twin screw pump, as opposed to centrifugal pumps is the capability of handling mixtures of liquid and vapour. In this report only twin screw pumps are considered.
The applications of screw pumps cover a diversified range of markets including navy, marine, and utilities fuel oil services; marine cargo; industrial oil burners; lubricating oil services; chemical processes; petroleum and crude oil industries; power hydraulics for navy and machine tools; and many others. The screw pump can handle liquids in a range of viscosities, from molasses to gasoline, as well as synthetic liquids in a pressure range from 3.5 to 350 *bar* and flows up to 1820 m^3/h. In this report only crude oil transportation is considered .
Because of relatively low inertia of their rotating parts, screw pumps are capable of operating at higher speeds than other rotary or reciprocating pumps of comparable displacement. Screw pumps, like other rotary positive displacement pumps, are self-priming and have a delivery flow characteristic, which is essentially independent of pressure, provided there is sufficient viscosity in the liquid being pumped.
Twin screw pumps are available in two configurations: single end and double end (see figure 1.2). Reference is made to [1] with respect to this chapter.

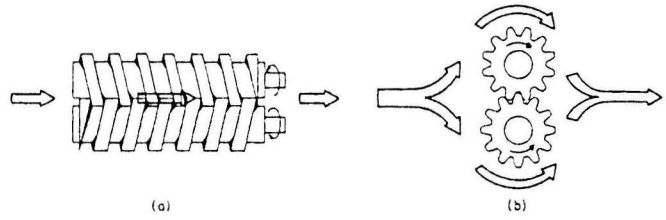

Figure 1.1: Diagrams of screw and gear elements, showing (a) axial and (b) circumferential flow

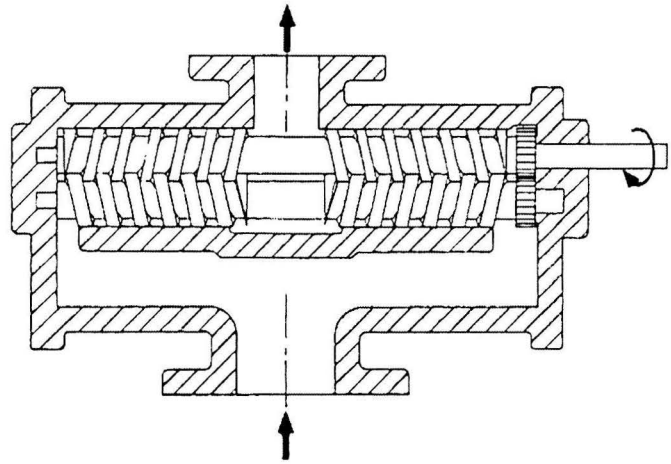

Figure 1.2: Twin screw pump with double-end arrangement and internal timing gears

1.1 Theory of screw pumps

In screw pumps, it is the intermeshing of the threads on the screws and the close fit of the surrounding housing (liner) that create one or more sets of moving seals in a series between the pump inlet and outlet. These sets of seals act as a labyrinth and provide the screw with its positive pressure capability. The successive sets of seals form fully enclosed cavities that move continuously from inlet to outlet, providing a smooth flow. Because the screw pump is a positive displacement device, it will deliver a definite quantity of liquid every revolution of the screws. This delivery can be defined in terms of displacement volume V_D, which is the theoretical volume displaced per revolution of the screws and is dependent only upon the physical dimensions of the screws. This delivery can also be defined in terms of theoretical capacity or flow rate Q_t measured in cubic meters per second, which is a function of displacement volume and speed N (rpm):

$$Q_t = \frac{1}{60} V_D N \tag{1.1}$$

If no internal clearances existed, the pump's actual delivered or net flow rate Q_r would equal the theoretical flow rate. Clearances, however, do exist with the result that whenever a pressure differential occurs, there will always be internal leakage from outlet to inlet. This leakage Q_l varies depending upon the pump type or model, the geometry of the clearance, the liquid viscosity, the rotation speed of the screws, and the differential pressure. The delivery flow rate or net flow rate is the theoretical flow rate minus the leakage flow rate: $Q_r = Q_t - Q_l$. If the differential pressure is almost zero, the leakage flow rate may be neglected and $Q_r = Q_t$. The theoretical flow rate is not dependent on the differential pressure over a positive displacement pump, see figure 1.3(a).

The theoretical flow rate of any pump can readily be calculated if all essential dimensions are known, see figure 1.3(b) for the screw dimension parameters. For any particular thread

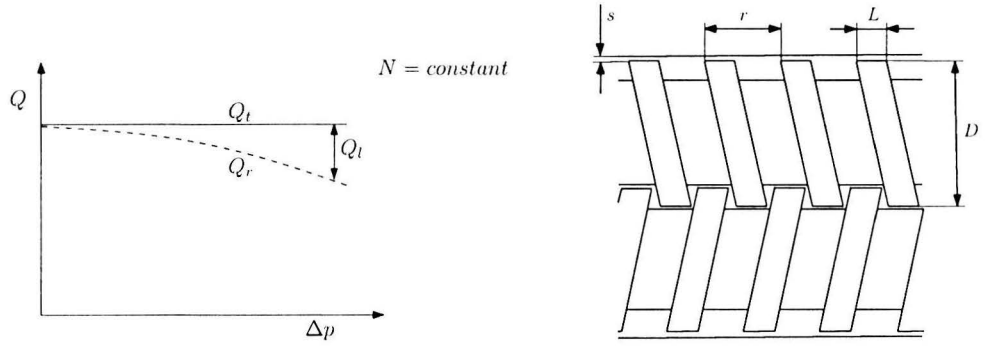

(a) Theoretic and realized volume flow rate against differential pressure for positive displacement pumps

(b) Parameters

Figure 1.3: Twin screw pump

configuration, assuming geometric similarity, the size of each cavity mentioned earlier is proportional to its length and cross-sectional area. The thread pitch r measured in terms of the same nominal diameter, which is used in calculating the cross-sectional area, defines the length. Therefore, the volume flow rate of each cavity is proportional to the cube of this nominal diameter and the speed of rotation N (rpm):

$$Q_t = kD^3N \tag{1.2}$$

or writing it in terms of pitch,

$$Q_t = k_1 \cdot r \cdot D^2N \tag{1.3}$$

where $r = kD/k_1$ with k and k_1 being constants.

Thus, for a given geometry, it can be seen that a relatively small increase in pump size can provide a large increase in flow rate. This is also true for centrifugal pumps which scale according to $\Phi = \frac{Q}{ND^3} = \text{constant}$. The theoretical flow rate of centrifugal pumps is influenced by the differential pressure over the pump, this is in contrast to positive displacement pumps like screw pumps.
The leakage flow rate can also be calculated, but it is usually estimated based on empirical values obtained from extensive testing. These test data are the basis of the design parameters used by every pump manufacturer. The leakage flow rate generally varies approximately with the square of the nominal diameter and linearly with the pressure difference. When neglecting the effect of rotation of the screws on the leakage flow rate, the net flow rate Q_r can be written as:

$$Q_r = kD^3N - k_2\Delta pD^2 \tag{1.4}$$

with k and k_2 empirical constants depending on the geometry and the working fluid.

1.2 Construction of screw pumps

Design concepts The pressure gradient in the pump elements of all the types of screw pumps produces various hydraulic reaction forces. The mechanical and hydraulic technique

employed for absorbing these reaction forces are one of the differences in the types of screw pumps produced by various manufacturers. Another fundamental difference lies in the method of engaging, or meshing, the screws and maintaining the running clearances between them. Two basic design approaches are used:

- The *timed screws* approach is based on an external means for phasing the mesh of the treads and for supporting the forces acting on the screws. In this concept, theoretically, the threads do no come into contact with each other nor with the housing bores in which they rotate.
- The *untimed screws* approach is based on the precision and accuracy of the screw forms for the proper mesh and transmission of rotation. They utilize the housing bores as journal bearings supporting the pumping reactions along the entire length of the screws.

Timed screw pumps require separate timing gears between the screws and separate support bearings at each end to absorb the reaction forces and maintain the proper clearances. Untimed screw pumps do not require gears or external bearings and thus are considerably simpler in design.

Double-end screw pumps The double-end arrangement is basically two opposed, single-end pumps or pump elements of the same size with a common driving screw that has an opposed, double-helix design with one casing. As can be seen from figure 1.2, the fluid enters a common inlet with a split flow going to the outboard ends of the two pumping elements and is discharged from the middle or center of the pumping elements. The two pump elements are, in effect, pumps connected in parallel. For low-pressure applications, the design can pump backwards when the direction of screw rotation is reversed. In either of these arrangements, all axial loads on the screws are balanced, as the pressure gradients in each end are equal and opposite. The double-end screw pumps construction is usually limited to low- and medium pressure applications, with 28 *bar* being a good practical limit to be used for planning purposes. Double-end pumps are generally employed where large flows are required or where highly viscous liquids are handled.

Timed design Timed screw pumps having timing gears and screw support bearings are available in two general arrangements: internal and external. The internal version has both the gears and the bearings located in the pumping chamber and the design is relatively simple and compact. This version is generally restricted to the handling of clean lubricating fluids, which serve as the only lubrication for the timing gears and bearings.
The external timing arrangement is the most popular and is extensively used. It has both the timing gears and screw support bearings located outside the pumping chamber. This type can handle a complete range of fluids, both lubricating and non-lubricating, and, with proper materials, has good abrasion resistance. The timing gears and bearings are oil-bath-lubricated from an external source. This arrangement requires the use of four stuffing boxes or mechanical seals, as opposed to the internal type, which employs only one shaft seal.
The main advantage of the timed screw pump is that the timing gears transmit power to the screws with no contact between the screw threads, thus promoting long pump life. The gears and screws are timed at the factory to maintain the proper clearance between the screws. The timing gears can be either spur or helical, herringbone, hardened-steel gears with tooth

profiles designed for efficient, quiet, positive drive of the screws. Antifrictional radial bearings are usually of the heavy-duty roller type, while the trust bearings, which position the screws axially, are either double-row, ball-thrust or spherical-roller types.
The housing can be supplied in a variety of materials, including cast iron, ductile iron, cast steel, stainless steel, and bronze. In addition, the screw bores of the housing can be lined with industrial hard chrome for abrasion resistance.
Since the screws are not generally in metallic contact with the housing or with one another, they can also be supplied in a variety of materials, including cast iron, heat-treated alloy steel, stainless steel, Monel, and nitralloy. The outside of the screws can also be covered with a variety of hard coating materials such as nickel based alloys, tungsten carbide, chrome oxide, or ceramic.

1.3 Special multiphase applications

Screw pumps have been used with gas-entrained application for many years, but recent process changes in oilfield technologies have created requirements for pumping multiphase fluids, containing more than just nominal amount of gases. In many oil well applications, the liquid oil flow eventually degenerates into all sorts of difficult multiphase mixtures of oil, gas, water, and sand. In the past, it was common for the gas to be separated and flared off at the well head with only the liquid product to be retained for further processing. If the gas is to be processed as well, separators, compressors, and dual pipelines are required to handle the gas phase. Therefore, a pump which can handle these difficult liquids with high gas contents, can save significant equipment costs as well as operating costs. Under various conditions, the well output can vary from 100 percent liquid to 100 percent gas, while maintaining the full discharge pressure.
When pumping multiphase products with high *gas void fractions*, the pump must be designed with a small pitch to provide a sufficient number of seals. The key to pumping multiphase products is to ensure that some liquid is always available to seal the screw clearances and reduce the leakage flow rate. Even a small amount of recirculated liquid is sufficient to provide this seal and enable the screw pump to operate with GVFs approaching 100 percent. Depending on a number of factors, the volume of liquid required to seal and cool the screws can be three to six percent of the total inlet volume flow rate. In order to ensure that sufficient liquid is available at conditions of high GVFs, a separate liquid flush can be provided or a separator type of body pump can be used. This type of body includes a special chamber that can separate some liquid from the multiphase mixture being pumped. This liquid can be recirculated back to the screws and mechanical seals to provide sealing and cooling liquid at times when the product is almost all gas.
When pumping liquids, the leakage flow rate through the internal clearances is proportional to the differential pressure and inversely proportional to the viscosity (assuming laminar flow through the clearances). However, in multiphase applications, as the void fraction increases, the leakage flow rate decreases. See figure 1.4(a) for the typical pump performance when pumping multiphase mixtures. Leakage flow compresses the gas in the upstream screw cavity. While the screw cavities move downstream, the gas void fraction reduces by the increased pressure. Some leakage flow fills the reduction in gas volume in the cavity, and a smaller leakage flow progresses to the next upstream cavity. This is clearly visible in figure 1.4(b). When the leakage flow rate is smaller, the differential pressure over a clearance is also smaller.

The leakage flow rate through the most upstream clearance is the total leakage flow rate of a twin screw pump for multiphase applications.

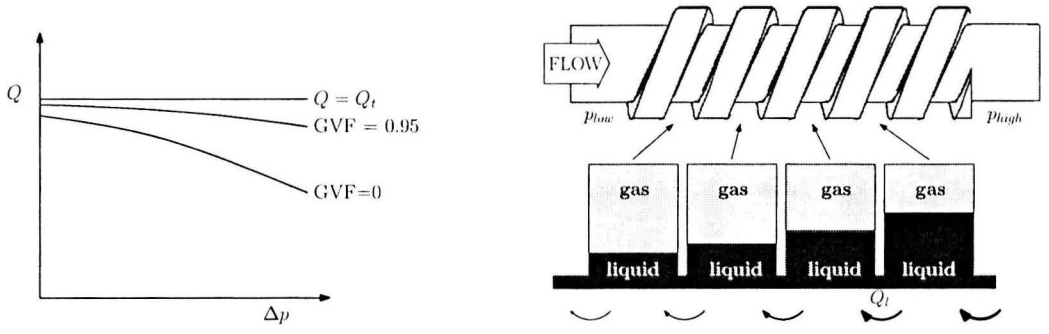

(a) Typical twin screw pump performance curve (N=constant)

(b) Gas compression by the leakage flow

Figure 1.4: Multiphase application of a twin screw pump

1.4 Goal and outline

The aim of the research is to predict the leakage flow rate of a multiphase twin screw pump by numerical simulations of the internal flow. This research can be divided in three stages: first, single phase flow in a non-rotating pump. Secondly, single phase flow in a rotating pump and thirdly, multiphase flow in a rotating pump. This report is restricted to the first stage and mainly focusses on the method to generate a suitable computational grid.

In chapter 2, the characteristics of the leakage flow are studied by considering two simpler cases: the flow through an annulus with rotating inner cylinder, and the flow through a straight-through labyrinth seal. Recommendations for the grid and turbulence model are given. In chapter 3, a method to create a three-dimensional grid of the screw pump and mesh methods for rotating screws is presented. It is used in chapter 4 to construct a three-dimensional grid of the twin screw pump. In chapter 5, the generated grid is used to simulate the leakage flow rate for non-rotating screws and single-phase flow with the three-dimensional grid. Finally in chapter 6, the conclusion of the developed mesh method and simulated leakage flow rate are discussed. Also recommendations to expand the model for time-dependent flow simulations and multiphase flow are discussed in this chapter.

Chapter 2

Simplified leakage flow in a twin screw pump

In section 2.1 the flow regime in the clearances of the screw is considered and the corresponding Reynolds number is estimated. The leakage flow in a twin screw pump is dependent on two phenomena. First, the leakage flow rate is dependent on friction in the small clearance between the tips of the rotating screw and the stationary liner. Secondly, the leakage flow rate is dependent on the flow resistance of the inlet and outlet of this clearance. These two phenomena in the leakage area of a twin screw pump are represented by two characteristic flow cases. First, the flow in an annulus with rotating inner cylinder. Secondly, flow through a stationary labyrinth seal. In section 2.2 the flow in an annulus with rotating inner cylinder is simulated for the corresponding Reynolds number of a twin screw pump. In section 2.3 the leakage flow through a stationary labyrinth seal is simulated for the corresponding Reynolds number of a twin screw pump. For the annulus with rotating inner cylinder and the labyrinth seal the simulated flow is compared with experimental results and recommendations for grid and turbulence model are given. In section 2.4 the simplified flow from section 2.1 and 2.2 is applied for a twin screw pump to estimate the leakage flow rate for a complete twin screw pump. In section 2.5 recommendations are made for the grid and turbulence model.

2.1 Reynolds number in twin screw pump

The Reynolds number is an important parameter for the flow regime. For pipe flow a Reynolds number smaller than 2100, based on hydraulic diameter and mean velocity, represents laminar flow and a higher Reynolds number represents turbulent flow in general. In the clearance area between screw and liner of a screw pump two directions of fluid motion are present. First the leakage flow in axial direction and secondly the tangential motion of fluid in the clearance. The axial Reynolds number Re and the tangential Reynolds number Re_ω are defined as:

$$Re = \frac{\langle v_{ax} \rangle \, s\rho}{\mu} \tag{2.1}$$

$$Re_\omega = \frac{\rho \omega R s}{\mu} \tag{2.2}$$

where $\langle v_{ax} \rangle$ is the mean axial flow velocity, R the outer screw radius, ω the angular velocity of the screw, s the clearance between screw and liner, ρ the density of the medium, and μ the dynamic viscosity. The axial Reynolds number is normally based on the hydraulic diameter $d_h = 2s$ but in equation (2.1) the notation of [11] is used. Note that with this notation a axial Reynolds number larger than 1050 represents turbulent flow in a pipe.
From these equations it is clear that the Reynolds numbers are dependent on dynamic viscosity and density of the medium, and the clearance. The tangential Reynolds number is dependent on the circumferential speed of the screw, while the axial Reynolds number depends on the axial velocity, which is in turn dependent on the differential pressure over the screw. The variables not concerning the geometry of the screw will be discussed point wise:
Viscosity A multiphase twin screw pump designed for pumping crude oil is considered. The dynamic viscosity of crude oil varies between $1.4 \cdot 10^{-3} - 20 \cdot 10^{-3}$ $kg/(ms)$ [1].
Tangential velocity The tangential velocity is dependent on the outer radius of the screw and the rotational speed of the screws. The maximum rotational speed typical for twin screw pumps designed for non-lubricating liquids is 1750 rpm [2] and for lubricating liquids 2900 rpm [3].
Axial velocity The mean axial leakage velocity for Hagen-Poiseuille flow in a cylindrical annulus is given in equation (2.3). This value of $\langle v_{ax} \rangle$ may serve as a first estimate since no axial movement of the annulus is taken into account. Also laminar flow is considered in this estimation. When the leakage flow is turbulent, the turbulent flow profile and the rotation of the screw produces deviations from this estimated mean axial velocity. Reference is made to [2] for this equation.

$$\langle v_{ax} \rangle = \frac{\Delta p s^2}{12 \mu L} \tag{2.3}$$

where L is the length of the annulus, Δp the pressure difference, s the clearance, and μ the dynamic viscosity.
With this mean axial velocity $\langle v_{ax} \rangle$ and the twin screw pump dimensions the axial Reynolds number can be estimated. The differential pressure over one seal is the total pressure build up divided by the number of seals, considering single phase flow. The total number of seals is dependent on the number of screw threads. In figure 2.1 a schematic view and a photograph of two screw threads are given. The cavities A and B in this figure are connected. To seal one cavity at least 2 screw threads are necessary, but normally just over 2 screw threads are used to ensure proper sealing. For example: $5\frac{1}{3}$ screw threads seal 4 cavities. Thus the typical total pressure build up over the pump is 16 bar [2] [3] at maximum. Assuming 4 seals, this gives a differential pressure Δp of 4 bar per seal.
The axial Reynolds number Re is estimated at 10,000 and the tangential Reynolds number Re_ω is 3000 for crude oil with the parameters given in table 2.1.
In this estimation of the axial Reynolds number the following phenomena are neglected:

- Axial flow profile is turbulent, resulting in an even higher axial velocity and Reynolds number.
- No inlet and outflow resistances are considered, and the axial velocity will be lower resulting in a lower axial Reynolds number.

[1] reference to http://www.engineeringtoolbox.com
[2] Houttuin 216.10 screw pump, http://houttuin.nl/contents/21610bro.pdf
[3] Houttuin 249.40 screw pump, http://houttuin.nl/contents/24940bro.pdf

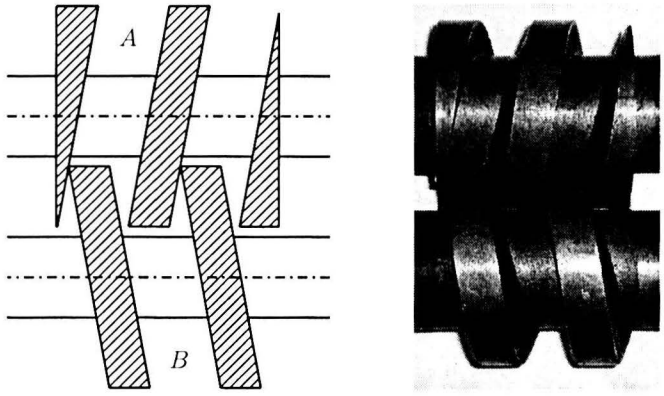

(a) Schematic view (b) Photograph

Figure 2.1: Two threads of twin screw pump

Table 2.1: Parameters for Reynolds numbers of a twin screw pump

μ	$1.4 \cdot 10^{-3}\ kg/(ms)$
ρ	$800\ kg/m^3$
N	$1350\ rpm$
Δp	$4\ bar$
L	$22\ mm$
R	$147\ mm$
s	$0.25\ mm$

- The screw translates opposite to the leakage flow, so the axial flow profile will be different. The mean axial velocity will be lower resulting in a lower axial Reynolds number. The axial screw velocity is given by $(N/60) \cdot r$, where N is the rotational speed in rpm, and r the screw pitch in m. The axial screw velocity is $1.35\ m/s$ at $1350\ rpm$ and a screw thread of $60\ mm$. This is low compared to the estimated mean axial velocity of $69.3\ m/s$.
- The screw rotates and this leads to a tangential motion of the fluid and, at high rotation speeds, to the occurrence of Taylor vortices in the fluid. This secondary flow leads to an additional resistance and a lower axial velocity and axial Reynolds number. In section 2.2 this rotation is considered.

2.2 Annulus with rotating inner cylinder

The resistance of a water flow in an annulus with a rotating inner cylinder is studied experimentally in [11]. For the CFD simulations, these experiments will serve as a test-case which will give recommendations for grid properties and turbulence model.

2.2.1 Experiment

The geometry of the test set-up used in [11] is given in figure 2.2. In this figure the fluid flows from left to right. The pressure is measured at three locations (N_I, N_{II} and N_{III}) and also the flow rate is measured. As is apparent from the figure, the pressure is measured at some distance from the inlet to minimize inlet flow effects. At every measuring location four holes of 0.4 mm in diameter and 90^o apart in the outer cylinder are connected to minimize measuring errors.
Anticipating a turbulent flow, the pressure drop Δp over the annulus is written as:

$$\frac{\Delta p}{\rho} = \left(\lambda \frac{L}{2s} + \delta_{io}\right) \frac{\langle v_{ax} \rangle^2}{2} \tag{2.4}$$

with λ the resistance coefficient, δ_{io} the resistance factor for the inlet and the outlet, L the axial length, s the clearance between inner and outer cylinder of the annulus, $\langle v_{ax} \rangle$ the mean axial velocity, and ρ the density. In figure 2.3, the resistance coefficient λ of various experiments with tangential Reynolds number Re_ω between 1000 and 20000 are given for axial Reynolds numbers Re in the range 100 to 25000. The axial Reynolds number for leakage flow in the clearances between screw and liner is more accurately estimated with equation 2.4. A δ_{io} of 1.5 is chosen according to [8] for the resistance of the in- and outlet. The axial Reynolds number is estimated at 2230.
For flow in an annulus with rotating inner cylinder, there are no inlet and outlet resistances, and δ_{io} is set to zero.

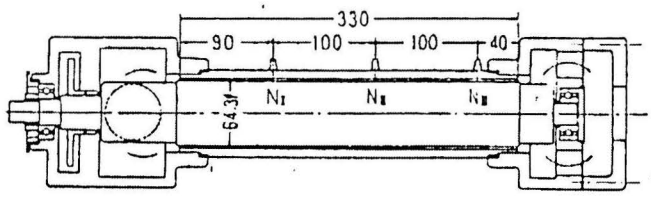

Figure 2.2: Experimental set-up of an annulus with rotating inner cylinder (dimensions in mm)

In table 2.2 the dimensions of the smallest annulus considered in the experimental study are given, and compared with typical dimensions of a screw pump. The clearance ratio s/R of a screw is much smaller than that of the annulus. It can be concluded that the clearance ratio does have an effect on the resistance coefficient λ (see figure 2.3). Therefore, the leakage flow rate of a screw pump can not be accurately determined from the measurements. However, this difference has no influence on recommendations for grid and turbulence model, because the exact geometry of the annulus is used in the numerical simulations.

2.2.2 Numerical simulation

For $Re = 2230$ and $Re_\omega = 3000$ a numerical simulation of flow in an annulus with rotating inner cylinder is performed with the commercial CFD-package Fluent. These Reynolds numbers indicate a turbulent flow. This is a steady axisymmetric problem, and is solved using

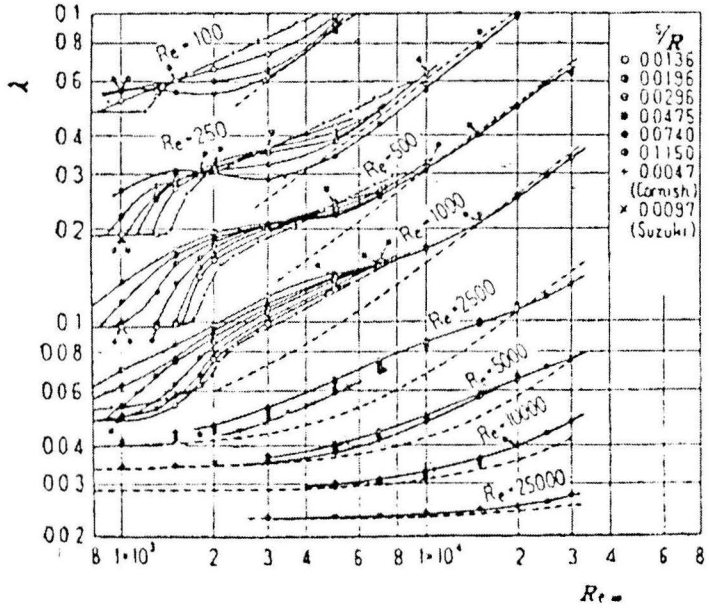

Figure 2.3: Relation between resistance coefficient λ and tangential Reynolds number Re_ω for various $\frac{s}{R}$ and axial Reynolds number Re

Table 2.2: Clearance ratio s/R for a twin screw pump and an annulus with rotating inner cylinder

	Radius R $[mm]$	Clearance s $[mm]$	Clearance ratio s/R [-]
Annulus	31.72	0.43	0.0136
Screw pump	147.25	0.25	0.0017

the segregated solver and implicit formulation. The segregated solver is used because in Fluent this solver is capable of adding multiphase models. The alternative, a coupled solver, is not capable of adding multiphase models. The coupled solver in Fluent solves the governing equations of continuity, momentum, and if necessary energy simultaneously as a set of equations. The segregated solver solves the governing equations sequentially (segregated from one another). The segregated solver can only be used with implicit formulation in Fluent. The continuity and momentum equations solved by the segregated solver are given in differential form and cylindrical coordinates as:

$$\frac{\partial \rho}{\partial t} + \frac{1}{r}\frac{\partial}{\partial r}(\rho r u_r) + \frac{1}{r}\frac{\partial}{\partial \theta}(\rho u_\theta) + \frac{\partial}{\partial z}(\rho u_z) = 0$$

$$\rho\left(\frac{\partial u_r}{\partial t} + u_r\frac{\partial u_r}{\partial r} + \frac{u_\theta}{r}\frac{\partial u_r}{\partial \theta} + u_z\frac{\partial u_r}{\partial z} - \frac{u_\theta^2}{r}\right) = -\frac{\partial p}{\partial r} - \left[\frac{1}{r}\frac{\partial}{\partial r}(r\tau_{rr}) + \frac{1}{r}\frac{\partial}{\partial \theta}\tau_{\theta r} + \frac{\partial}{\partial z}\tau_{zr} - \frac{\tau_{\theta\theta}}{r}\right]$$

$$\rho\left(\frac{\partial u_\theta}{\partial t}+u_r\frac{\partial u_\theta}{\partial r}+\frac{u_\theta}{r}\frac{\partial u_\theta}{\partial \theta}+u_z\frac{\partial u_\theta}{\partial z}-\frac{u_r u_\theta}{r}\right)=-\frac{1}{r}\frac{\partial p}{\partial \theta}-\left[\frac{1}{r^2}\frac{\partial}{\partial r}(r^2\tau_{r\theta})+\frac{1}{r}\frac{\partial}{\partial \theta}\tau_{\theta\theta}+\frac{\partial}{\partial z}\tau_{z\theta}\right]$$
$$\rho\left(\frac{\partial u_z}{\partial t}+u_r\frac{\partial u_z}{\partial r}+\frac{u_\theta}{r}\frac{\partial u_z}{\partial \theta}+u_z\frac{\partial u_z}{\partial z}\right)=-\frac{\partial p}{\partial z}-\left[\frac{1}{r}\frac{\partial}{\partial r}(r\tau_{rz})+\frac{1}{r}\frac{\partial}{\partial \theta}\tau_{\theta z}+\frac{\partial}{\partial z}\tau_{zz}\right] \quad (2.5)$$

where ρ is the density, u the fluid velocity, τ the shear tensor, and p the pressure. The term $\frac{\partial}{\partial \theta}$ is zero for axisymmetric problems. In case of steady state calculations the $\frac{\partial}{\partial t}$ term is also zero. The equations of continuity and momentum are implemented in the SIMPLE method (Semi Implicit Method for Pressure Linked Equations). This method calculates the flow field with an estimate of the pressure. After this, the pressure is corrected with the solution of the flow field to form a new estimate of the pressure. In this way iteratively a solution for the flow field and the pressure can be calculated that satisfies both continuity and momentum equations. The equations of the SIMPLE method are solved with the Gauss-Seidel algorithm for an Algebraic MultiGrid (AMG). Discussing these methods falls outside the scope of this report. In [4] and [7] these methods are discussed.
Numerical models have two approaches to model turbulent flow behaviour near solid walls; wall functions and near-wall modeling approaches. Wall functions use semi-empirical formulas to resolve the flow in large cells near the wall. Near-wall modeling uses small cells near the wall to resolve the flow. The approaches each have different requirements on the size of the first cell at the wall. This is expressed in the dimensionless wall distance y^+, defined as:

$$y^+ \equiv \rho u_\tau y/\mu \quad (2.6)$$

where y is the distance of the center of the element to the wall, μ the dynamic viscosity and u_τ the friction velocity given by $\sqrt{\frac{\tau_w}{\rho}}$ where τ_w is the wall-shear stress defined as $\tau_w = \mu\left(\frac{\partial u}{\partial y}\right)_{y=0}$. The required y^+ for the wall function approach is $30 < y^+ < 200$. A value closer to the lower bound is most desirable. The required y^+ for near-wall modeling is of the order of 1. The upper bound is $y^+ < 4 \sim 5$. Another criterion for near-wall modeling is that there are at least 10 cells within the viscosity-affected boundary layer. In [4] en [6] these methods are discussed extensively.

In the remainder of this section, numerical results will be compared with results from experiments as given in figure 2.3. Values of resistance coefficient λ at intermediate Reynolds numbers are determined by linear interpolation. In the simulations, two near-wall approaches will be considered: first wall functions will be evaluated, and secondly near-wall modeling.

Wall functions

With the $k-\epsilon$ model with standard wall functions, the value of y^+ is calculated for grids with different number of cells in radial direction. The value of y^+ is solution dependent: it will vary slightly for different turbulence models, but it gives a good idea of the dimensionless wall distance with that grid. In table 2.3 the dimensionless wall distance is given for different number of cells n_{cell} in radial direction. The required dimensionless wall distance $30 < y^+ < 200$ is not reached with these Reynolds numbers ($Re = 2230$ and $Re_\omega = 3000$). The calculated resistance coefficient does not seem to be influenced much by the dimensionless wall distance. To maintain some radial cells in the annulus and to keep the value of y^+ close to the required value, $n_{cell} = 5$ is chosen to determine the accuracy of the different turbulence models.

Table 2.3: Dimensionless wall distance y^+ and resistance coefficient λ for different grids of the annulus problem determined with the standard $k-\epsilon$ model and standard wall function ($Re = 2230, Re_\omega = 3000$)

n_{cell}	y^+	λ_{num}
4	22	0.0455
5	18	0.0461
6	15	0.0464
7	13	0.0466
8	11	0.0466

In table 2.4 the calculated resistance coefficient λ is given for the $k-\epsilon$ and $k-\omega$ turbulence models with various model options and wall functions. Furthermore, the difference between the calculated and the experimental value of the resistance coefficient λ is given. A structured grid with equilateral edges is used, see figure 2.5(a). The axial length of the structured elements is not considered of importance due to the axial nature of the flow. Additional numerical simulations with elongated cells in axial direction (2, 5 and 10 times) give the same resistance coefficients λ.

Table 2.4: Resistance coefficient λ for various turbulence models with wall functions determined for the annulus problem ($n_{cell} = 5, y^+ = 18$, $\lambda_{exp} = 0.0579, Re = 2230, Re_\omega = 3000$)

turb. model	version	option	wall function	λ_{num}	dev [%]
$k-\epsilon$	standard		standard	0.0461	20.4
			non-equilibrium	0.0477	17.6
	RNG		standard	0.0447	22.8
			non-equilibrium	0.0463	20.0
		differential	standard	0.0421	27.3
			non-equilibrium	0.0442	23.7
		swirl	standard	0.0442	23.7
			non-equilibrium	0.0459	20.7
		diff+swirl	standard	0.0419	27.6
			non-equilibrium	0.0422	27.1
	realizable		standard	0.0452	21.9
			non-equilibrium	0.0469	19.0
$k-\omega$	standard			0.0554	4.3
		shear flow corr.		0.0544	6.0
	SST			0.0553	4.5

The $k-\omega$ turbulence models are most accurate in this situation. In figure 2.4 the y^+-dependency for the Standard and SST $k-\omega$ model is given, using grids with different values of n_{cell}. Also the results for the standard $k-\epsilon$ turbulence model are given in this figure.

The dependency on y^+ is obvious, over prediction for low y^+ values and under prediction for higher y^+ values, for the $k-\omega$ turbulence model. Still, these models can be used because the deviation is smaller than with the $k-\epsilon$ models. In [6] this dependency on y^+ was also mentioned for $k-\omega$ turbulence models.

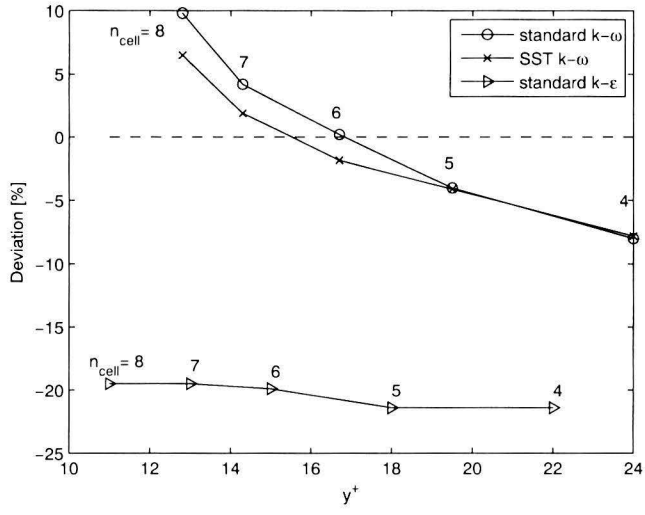

Figure 2.4: Relation between deviation of calculated and experimental resistance coefficient λ for different y^+ values for the annulus problem ($Re = 2230, Re_\omega = 3000$, standard wall function)

The standard $k-\omega$ model is used to calculate the resistance coefficient for different axial and tangential Reynolds numbers. The deviation with the experimental results and the dimensionless wall distance are given in table 2.5. There is a high deviation at $y^+ = 10.5$ which could be explained by the linear (laminar) law that Fluent employs for turbulent boundary layers at approximately $y^+ < 11$.

Table 2.5: Resistance coefficient λ for different Re combinations with standard $k-\omega$ model and wall functions ($n_{cell} = 6$)

Re	Re_ω	y^+	λ_{num}	λ_{exp}	dev [%]
1000	2000	10.5	0.105	0.076	38
	3000	12	0.112	0.098	14
	6000	17	0.135	0.152	11
2500	2000	17	0.0522	0.0457	14
	3000	18	0.538	0.543	1
	6000	21	0.0616	0.068	9

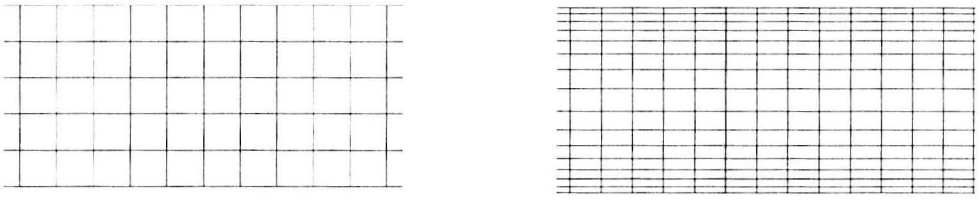

(a) wall function ($n_{cell} = 5$) (b) near-wall modeling ($n_{cell} = 15$)

Figure 2.5: Partial mesh of the annulus with rotating inner cylinder for different wall approaches

Near-wall modeling

Similar to the previous section, first the dimensionless wall distance will be calculated for different grids, while keeping in mind that the total number of cells should be kept as low as possible. Three different grids are considered, n_{cell} equal to 10, 15 and 20 and a smooth grid refinement towards the solid walls (figure 2.5(b)). In table 2.6 the corresponding y^+ values of the different grids are given. For $Re = 2230$ and $Re_\omega = 3000$ the dimensionless wall distance with $n_{cell} = 10$ is too high. Another criterion states that there are at least 10 cells in the viscosity affected region [4]. This would bring the total number of cells up, so simulations are performed to test this criterion. For $n_{cell} = 15$ the resistance coefficient is determined for the different turbulence models with near-wall modeling, results are given in table 2.7.

Table 2.6: Dependency of dimensionless wall distance y^+ for different grids determined with standard $k - \omega$ turbulence model and near-wall modeling for the annulus problem

n_{cell}	y^+	λ_{num}
10	7	0.0517
15	3.2	0.0548
20	1.7	0.0632

2.3 Labyrinth seal

Leakage flow in a twin screw pump has a stream path that is similar to the stream path through a 'straight-through labyrinth seal'. The results of numerical simulations are compared with the experimental results to give recommendations for the grid and turbulence model.

2.3.1 Experimental set-up

Airflow through a stationary straight-through labyrinth seal is studied experimentally in [5]. In this study, air flows through the seal with axial Reynolds numbers in a range of 300 to 7500 in the seal clearance. In figure 2.6 a schematic view of the labyrinth seal is given. In table

Table 2.7: Resistance coefficient λ for various turbulence models with near-wall modeling for the annulus problem ($n_{cell} = 15, y^+ = 3, \lambda_{exp} = 0.0579, Re = 2230, Re_\omega = 3000$)

turb. model	version	option	λ_{num}	dev. [%]
$k-\epsilon$	standard		0.0572	1.2
	RNG		0.0573	1.0
		differential	0.0578	0.2
		swirl	0.0574	0.9
		diff+swirl	0.0578	0.2
	realizable		0.0578	0.2
$k-\omega$	standard		0.0548	5.4
		shear flow corr.	0.0506	12.6
	SST		0.0543	6.2

2.8 the dimensions of the labyrinth seal and the twin screw pump are given. The clearance s and the diameter of the labyrinth seal D are similar to the screw pump, the length of the clearance L and the pitch r are considerably smaller than for the screw pump. Inlet and outflow resistances are the main sealing principle of a labyrinth seal. For a twin screw pump the sealing between screw cavities is also established by a relatively long sealing clearance. The total leakage flow rate of the screw pump can not be estimated directly with the leakage flow rate through the labyrinth seal, because of this difference in sealing principle and the non-rotating seal. The larger sealing length of the clearance has to be taken into account to estimate the leakage flow rate in a screw pump. However, this difference has no influence on recommendations for grid and turbulence model.

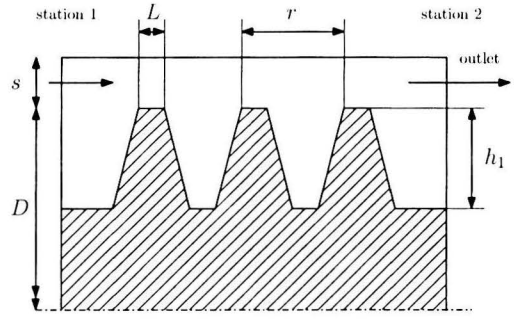

Figure 2.6: Experimental set-up of straight-through labyrinth seal

		Labyrinth seal	Twin screw pump
s	$[mm]$	0.36	0.25
D	$[mm]$	356	295
L	$[mm]$	0.25	22
r	$[mm]$	6	60
h_1	$[mm]$	6	85

Table 2.8: Dimensions of straight-through labyrinth seal and twin screw pump

2.3.2 Numerical simulation

A numerical simulation in Fluent is performed to calculate the mass flow rate through the labyrinth seal for Re equal to 1572 and 2195. The Mach number Ma is a measure for the variation of density, according to $Ma^2 \propto \Delta p$. A density variation smaller than ten percent is present here, and compressibility is neglected in the numerical simulation. Different turbu-

Table 2.9: Experimental results labyrinth seal

p_1 $[kPa]$	p_2 $[kPa]$	$\dot{m}$ $[kg/s]$	ρ $[kg/m^3]$	Re [-]	Ma [-]
100.695	92.503	0.027303	1.1738	1572	0.20
108.793	93.806	0.038118	1.2680	2195	0.28

lence models are evaluated with the grid given in figure 2.7. This is a structured quadrilateral grid with 5 radial cells in the seal clearance. In Fluent a steady axisymmetric problem is solved with the segregated solver and implicit formulation using standard wall function for incompressible flow. Anticipating the results presented in chapter 3, it is concluded that the number of cells should be kept as low as possible. Therefore, only wall functions are considered for the simulation of flow through a labyrinth seal. In table 2.10 the calculated mass flow rate and the deviation with the experimental mass flow rate is given. The flow through the labyrinth seal results in a vortex in the seal cavity, which is clearly visible at the streamlines of the flow in the labyrinth seal, given in figure 2.8.

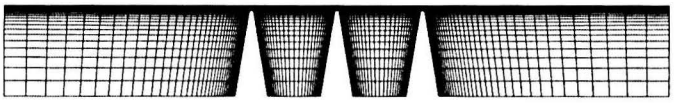

Figure 2.7: Structured quadrilateral grid of straight-through labyrinth seal

Table 2.10: Mass flow rate in a stationary labyrinth seal for various turbulence models using wall functions

		$Re = 1572, y^+ > 11,$ $\dot{m} = 0.0273$		$Re = 2195, y^+ > 14,$ $\dot{m} = 0.0381$	
		$\dot{m}$ $[kg/s]$	dev [%]	$\dot{m}$ $[kg/s]$	dev [%]
$k-\epsilon$	Standard	0.0281	2.9	0.0399	4.7
	RNG	0.0294	7.7	0.0421	10.4
	Realizable	0.0299	9.5	0.0428	12.3
$k-\omega$	Standard	0.0267	2.2	0.0379	0.6
	SST	0.0304	11.4	0.0437	14.6

2.4 Leakage flow in twin screw pump

The flow through an annulus gives an idea of the leakage flow rate in the clearances between the screw and the liner of a screw pump. In this section the leakage flow is estimated with the method to calculate the mean axial flow through a stationary annulus and an annulus with rotating inner cylinder. The difference in clearance ratio s/R between the twin screw pump and the annulus with rotating inner cylinder is neglected.

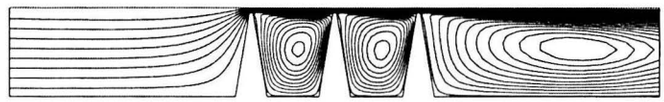

Figure 2.8: Streamlines of the flow in a straight-through labyrinth seal

The leakage flow rate through the clearance between screw and liner Q_{cl} of a twin screw pump is approximately given by the following equations:

$$Q_{cl} = \langle v_{ax} \rangle A_{cl} \tag{2.7}$$

$$A_{cl} = \left(4\pi - 4\cos\left(\frac{h/2}{R}\right)\right) Rs \tag{2.8}$$

where h is the distance between the centers of the screws, s the clearance between screw and liner, R the outer radius of the screw, and A_{cl} the projected area of the clearance on a plane perpendicular to the axial direction.
The ratio between the total leakage flow rate and the theoretical pumped volume flow rate of a screw is an important pump performance parameter. The leakage flow rate through the clearance between screw and liner is part of the total leakage flow, and is considered in the ratio Q_{cl}/Q_t. For the theoretical flow rate Q_t reference is made to chapter 1. The theoretical volume flow rate is given by:

$$Q_t = \frac{1}{60} V_D N \tag{2.9}$$

$$V_D = (A_{liner} - 2 \cdot A_{screw}) \cdot r \tag{2.10}$$

where N is the rotational speed of the screws in rpm, V_D the displacement volume for one revolution, r the screw pitch, A_{screw} the area of the cross-section of the screw, A_{liner} the area of the cross-section of the liner.
The displacement volume V_D for the screw is determined by the dimensions of the screw and liner. For the screw given in appendix B, the $A_{screw} = 37 \cdot 10^{-3} m^2$, and $A_{liner} = 124 \cdot 10^{-3} m^2$. This gives a displacement volume V_D of $3 \cdot 10^{-3}\ m^3/rev$.

The leakage flow rate in a twin screw pump is estimated in three ways. First, using equation (2.3) assuming laminar leakage flow through a stationary seal without inlet and outlet resistances. Secondly, using equation (2.4) for a turbulent leakage flow through an annulus with rotating inner cylinder, also without inlet and outlet resistances. Thirdly, using equation (2.4) for a turbulent leakage flow through an annulus with rotating inner cylinder, now with a value of 1.5 for the inlet and outlet resistance δ_{io}. For the annulus with rotating inner cylinder an iterative procedure is applied, since the resistance coefficient λ depends on axial Reynolds number, and thus on the leakage flow rate. In table 2.11 the leakage flow rate is given for the different methods.

Table 2.11: Estimated leakage flow of oil through a twin screw pump (app. B) for $Re_\omega = 3000, \Delta p = 4\ bar, N = 1350\ rpm$

	$\langle v_{ax} \rangle$	Re	Q_t	Q_{cl}	Q_{cl}/Q_t
	$[m/s]$	[-]	$[m^3/s]$	$[m^3/s]$	[%]
stationary + laminar	69.3	10,000	0.0675	0.0246	36.4
rotating + turbulent	22.3	3220	0.0675	0.0079	11.7
rotating + turbulent + inlet/outlet losses	15.7	2230	0.0675	0.0056	8.3

2.5 Conclusion

The leakage flow in the clearance between screw and liner of a twin screw pump is dependent on two phenomena. First, the leakage flow rate is dependent on friction in the small clearance between the tips of the rotating screw and the stationary liner. Secondly, the leakage flow rate is dependent on the flow resistance of the inlet and outlet of this clearance. These two phenomena in the leakage area of a twin screw pump are represented by two characteristic flow cases. First, the flow in an annulus with rotating inner cylinder. Secondly, flow through a stationary labyrinth seal. The axial Reynolds number in the clearance is determined by the flow in an annulus. Anticipating the results as presented in chapter 3 it is concluded that the number of radial cells must be limited and that near-wall modeling is not preferable.

The $k - \omega$ turbulence model performs best for the flow in an annulus with rotating inner cylinder using wall functions, and performs good for the flow in an annulus using near-wall modeling. The standard $k - \omega$ and standard $k - \epsilon$ turbulence model perform best for the flow in a labyrinth seal. In [6], the flow phenomena in an internal combustion chamber were represented by two characteristic flow cases: the backward facing step and the free jet flow. Based on different grid refinements and different turbulence models, it was concluded that the standard $k - \omega$ model performs good, but has a grid dependency. In this study, however, it is shown that this dependency has little effect on the accuracy to represent the leakage flow rate in an annulus with rotating inner cylinder.

The $k - \epsilon$ turbulence model performs best for flow in an annulus using near-wall modeling.

Near-wall modeling is not preferred, and the standard $k - \omega$ turbulence model with wall functions is preferred for the simulation of flow in a twin screw pump.

The axial Reynolds number in the clearance between screw and liner is estimated in three ways. First, considering laminar flow in a stationary annulus with rotating inner cylinder without inlet and outlet resistances. Secondly, considering turbulent flow in an annulus with rotating inner cylinder without inlet and outlet resistances. Thirdly, turbulent flow in an annulus with rotating inner cylinder with inlet and outlet resistances. The axial Reynolds number reduces when rotation and inlet and outlet resistances are considered.

Chapter 3

Method of three-dimensional meshing

In chapter 2, two-dimensional leakage flow in screw pumps is discussed. For three-dimensional flow calculations the number of cells can be very high. The calculation time is dependent on the number of cells used to simulate the flow in a screw pump. Therefore, a limited number of cells is desirable. Furthermore the quality of the grid has to be acceptable to perform meaningful flow calculations. In the first section of this chapter the number of cells for an unstructured, and a structured grid is estimated assuming cells with perfect quality (based on skewness). A time-dependent simulation of flow in a twin screw pump requires the screws to rotate, thereby the cavities between the screws progress to the pump outlet. This requires a dynamic mesh. Methods for a dynamic mesh are discussed in section 3.2. While the screws are rotating, the inlet and outlet remain stationary. This could give problems connecting those regions if nodes should always coincide. A non-conformal grid does not require that nodes coincide on the combined faces. This is discussed in section 3.3. Finally, recommendations are made to set-up a time-dependent simulation of a screw pump in section 3.4.

3.1 Number of cells in the clearance region

The number of cells in the clearance region of a screw pump is estimated because the axial distance L of the clearance is high compared to the radial distance s of the clearance between screw and liner. Therefore, the number of cells in the clearance constitutes a substantial part of the total number of cells to describe a complete twin screw pump. First the number of cells in the clearance is estimated in case an unstructured tetrahedral mesh is used. After this, the number of cells is estimated in case a structured mesh is used. The approximate volume of the clearance region (figure 3.1(a)) is given by the following equation:

$$V_{cl} = n_{rev} L A_{cl} \tag{3.1}$$

where n_{rev} is the number of screw threads, L the (axial) screw thickness, and A_{cl} the cross-sectional area of the clearance, given in equation (2.8).
In an unstructured tetrahedral mesh of high quality, all cells are truly tetrahedral with edges of equal length. The volume of such a regular tetrahedral cell V_{tet} is given by:

$$V_{tet} = \frac{1}{12} a^3 \sqrt{2} \tag{3.2}$$

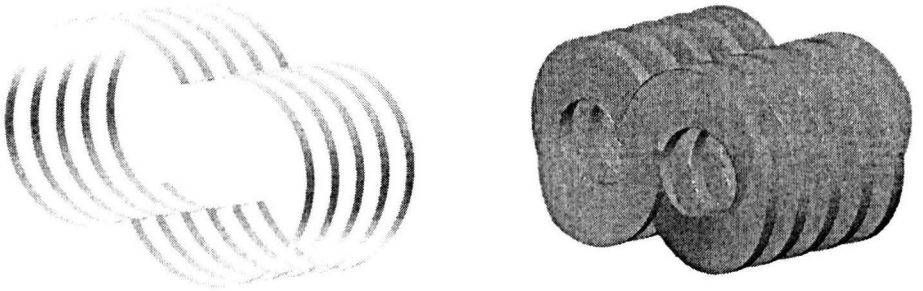

(a) Clearance between screw and liner (b) 5 threads of the screws

Figure 3.1: Twin screw pump

where a is the edge length of the cell. The length a is determined from the required number of cells in radial direction from screw to liner, n_{cell}. The height h of a regular tetrahedral cell is $h = \frac{a}{3}\sqrt{6}$. In figure 3.2 the height h is given by $h = \frac{s}{n_{cell}}$. This gives the following expression for a:

$$a = \frac{3s}{\sqrt{6}\, n_{cell}} \tag{3.3}$$

The estimated number of unstructured cells in the clearance between screw and liner is given by:

$$n_{unstr} = \frac{V_{cl}}{V_{tet}} = \frac{n_{rev} L A_{cl}}{\frac{1}{12} a^3 \sqrt{2}} \tag{3.4}$$

With a from equation (3.3), and $n_{cell} = 5$ according to chapter 2, the number of unstructured cells in the clearance n_{unstr} is approximately $1.5 \cdot 10^9$ cells for a twin screw pump. The global dimensions of the twin screw pump are given in table 2.1 and in appendix B a complete drawing of the twin screw pump is given.

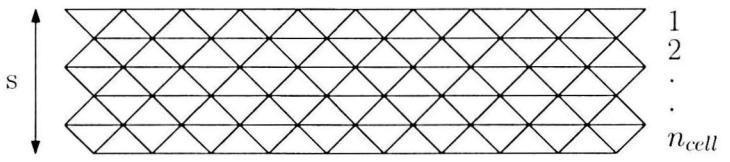

Figure 3.2: Triangular cells in clearance between screw and liner

The number of structured cells in the clearance between screw and liner is estimated, similar to the unstructured case. The skewness of structured hexahedral cells is not affected by the aspect ratio of the edges of the cell f_{AR}. In figure 3.3 the structured mesh is given.
The volume of a hexahedral cell is given by:

$$V_{hex} = \frac{a^3}{f_{AR}} \tag{3.5}$$

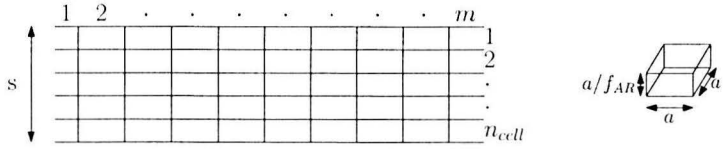

Figure 3.3: Hexahedral cells in clearance between screw and liner with aspect ratio f_{AR}

The length a of the edge of a cell is determined by clearance s, the number of cells in radial direction across the clearance, n_{cell}, and the chosen value for the aspect ratio f_{AR}. The length a is then given by:

$$a = \frac{s\ f_{AR}}{n_{cell}} \tag{3.6}$$

The estimated number of structured cells in the clearance between screw and liner is given by:

$$n_{str} = \frac{V_{cl}}{V_{hex}} = \frac{n_{rev} b A_{cl} f_{AR}}{a^3} \tag{3.7}$$

With a from equation (3.6), V_{cl} from equation (3.1), $f_{AR} = 10$, and $n_{cell} = 5$, the number of unstructured cells in the clearance n_{str} is approximately $3.3 \cdot 10^6$ cells.

3.2 Dynamic mesh

In this section the distortion of the mesh is considered. In Fluent a dynamic mesh can be achieved by repositioning of nodes. The nodes can be repositioned by smoothing, dynamic layering and remeshing. Another dynamic mesh method is the use of ALE-calculations, this is not a method to reposition the nodes. ALE-calculations are a method to perform calculations on cells with nodes moving in time, while maintaining the grid topology. Still an initial mesh has to be generated before repositioning and ALE-calculations can be performed. For ALE-calculations, grids have to be generated with the same grid topology for every time step.

3.2.1 Smoothing

In the **spring based smoothing**, the edges between any two mesh nodes are idealized as a network of interconnected springs. The initial spacings of the edges before any boundary motion constitute the equilibrium state of the mesh. A displacement at a given boundary node will generate a force proportional to the displacement along all the springs connected to the node. For non-tetrahedral cell zones (non-triangular in 2D), the spring-based method is recommended when the following conditions are met:

- The boundary of the cell zone moves predominantly in one direction (i.e., no excessive anisotropic stretching or compression of the cell zone).
- The motion is predominantly normal to the boundary zone.

If these conditions are not met, the resulting cells may have high skewness values, since not all possible combinations of node pairs in non-tetrahedral cells (or non-triangular in 2D) are idealized as springs.
Laplacian smoothing is the most commonly used and the simplest mesh smoothing method. This method adjusts the location of each mesh node to the geometric center of its neighboring nodes. This method is computationally inexpensive but it does not guarantee an improvement on mesh quality, since repositioning a node by Laplacian smoothing can result in poor quality elements. To overcome this problem, Fluent only relocates the node to the geometric center of its neighboring nodes if and only if there is an improvement in the mesh quality (i.e., the skewness has been improved).

3.2.2 Dynamic layering method

In prismatic (hexahedral and/or wedge) mesh zones, one can use dynamic layering to add or remove layers of cells adjacent to a moving boundary, based on the height of the layer adjacent to the moving surface. The dynamic mesh model in Fluent allows to specify an ideal layer height on each moving boundary. The layer of cells adjacent to the moving boundary is split or merged with the layer of cells next to it based on the height of the cells in layer attached to the moving boundary.

3.2.3 Remeshing

On zones with a triangular or tetrahedral mesh, the spring-based smoothing method is normally used. When the boundary displacement is large compared to the local cell sizes, the cell quality can deteriorate or the cells can become degenerate. This will invalidate the mesh (e.g., result in negative cell volumes) and consequently, will lead to convergence problems when the solution is updated to the next time step. To circumvent this problem, Fluent agglomerates cells that violate the skewness or size criteria and locally remeshes the agglomerated cells or faces. If the new cells or faces satisfy the skewness criterion, the mesh is locally updated with the new cells (with the solution interpolated from the old cells). Otherwise, the new cells are discarded. Fluent includes several remeshing methods that include local remeshing, local face remeshing (for 3D flows only), face region remeshing, and 2.5D surface remeshing (for 3D flows only). The available remeshing methods in Fluent work for triangular-tetrahedral zones and mixed zones where the non-triangular/tetrahedral elements are skipped. The exception is the 2.5D model, where the available remeshing method only work on wedges extruded from triangular surfaces.
Using the **Local remeshing method**, Fluent marks cells based on cell skewness and minimum and maximum length scales as well as an optional sizing function. Fluent evaluates each cell and marks it for remeshing if it meets one or more of the following criteria:

- It has a skewness that is greater than a specified maximum skewness.
- It is smaller than a specified minimum length scale.
- It is larger than a specified maximum length scale.
- Its height does not meet the specified length scale (at moving face zones, e.g., above a moving piston).

Face region remeshing method
In addition to remeshing the volume mesh, Fluent also allows triangular and linear faces on a deforming boundary to be remeshed. Fluent marks deforming boundary faces for remeshing based on moving and deforming loops of faces. For face region remeshing, Fluent marks the region of faces on the deforming boundaries at the moving boundary based on minimum and maximum length scales. Once marked, Fluent remeshes the faces and the adjacent cells to produce a very regular mesh on the deforming boundary at the moving boundary.

3.2.4 Arbitrary Lagrangian-Eulerian calculations (ALE)

The Arbitrary Lagrangian-Eulerian method is a method allowing time-dependent CFD. It is a mix between the Lagrangian and the Eulerian methods.
The Lagrangian method is a time-dependent CFD method in which the calculation grid moves with the local fluid velocity. It has a particular advantage that advective terms effectively disappear in the flow equations. It is however severely limited by tangling of the grid in multidimensional problems, especially when vortices occur.
In the Eulerian method, the calculation grid is stationary. It obviously is not hampered by tangling grids, but is incapable of representing moving domain boundaries.
The ALE method is a mix of both methods in that it allows the grid to move with a velocity that is independent of the flow solution. The only limitations are the need to have a valid grid at each time step, and the restriction that the grid topology must be maintained. The latter means that the only allowed action on the grid is a free movement of the nodes.
To discretize the Navier-Stokes equations in ALE-formulation with a finite-volume technique, the velocity of the boundaries of the control volumes $\mathbf{u}_b$ must be known for each time step. The boundary velocity can be calculated from the position of the nodes at subsequent time steps separately from the Navier-Stokes equations. At the present, commercial CFD packages are available that can handle ALE calculations. In equation (3.8) the Navier-Stokes equations are given. Reference is made to [10] for these equations.

$$\begin{aligned}
&\text{geometric conservation law} && \frac{\partial}{\partial t}\left(\oint_{\Omega} dV\right) - \oint_{\partial\Omega} \mathbf{u}_b \cdot d\mathbf{S} = 0, \\
&\text{conservation of mass} && \frac{\partial \rho}{\partial t} + \frac{\partial}{\partial \mathbf{x}}(\rho(\mathbf{u} - \mathbf{u}_b)) = 0, \\
&\text{conservation of momentum} && \frac{\partial \rho \mathbf{u}}{\partial t} + \frac{\partial}{\partial \mathbf{x}}(\rho \mathbf{u}(\mathbf{u} - \mathbf{u}_b) - \tau) + \frac{\partial p}{\partial \mathbf{x}} = 0,
\end{aligned} \tag{3.8}$$

where ρ is the density, $\mathbf{u}_b$ the velocity vector of the cell boundary, $\mathbf{u}$ the fluid velocity vector, τ the shear tensor, and p the pressure.
For the twin screw pump this ALE-method has a particular advantage. The positioning of the nodes only has to be performed once for one screw thread. Rotation of the screws equals axial displacement of the grid. The last layers can be removed and added to the front to complete the grid. More screw threads are easily added due to periodicity, this is also applicable for the initial grid of other meshes.

3.3 Non-conformal mesh

While the screws are rotating, the inlet and outlet remain stationary. Connecting those regions could give problems if nodes should always coincide. A non-conformal grid does not require that nodes coincide on the combined faces. In Fluent it is possible to use a grid composed of cell zones with non-conformal boundaries. That is, the grid node locations need not to be identical at the boundaries where two subdomains meet. Fluxes across the grid interface are computed using the faces resulting from the intersection of the two interfaces, not from the two interfaces separately.

3.4 Conclusion

From the estimation of the number of cells in the clearance between screw and liner, an unstructured mesh of the clearances between screw and liner is impossible due to the large number of needed cells. The total number of cells to describe the twin screw pump has to be less than a few million cells, to be solvable with normal PC performance and memory. The clearance between screw and liner can be represented with structured hexahedral cells. The aspect ratio of the hexahedral cell has to be larger than 10 to make a model of the total twin screw pump with a few million cells. The inlet and outlet of the pump can be connected with a non-conformal mesh interface, or special care has to be taken to make the nodes at the interface coincide. To develop a dynamic mesh, smoothing and remeshing can be used, even when the topology of the mesh changes in time. ALE-calculations for a dynamic mesh, without change in topology, are preferred above smoothing and remeshing because of the lower demands on PC performance. ALE-calculations are performed for twin screw compressor in [9], so this method is considered feasible for a twin screw pump.

Chapter 4

Construction of structured grid

For a CFD calculation of a twin screw pump, the need for a structured grid is twofold. First the number of elements needs to be kept within limits and secondly the quality of the grid needs to be well controlled. To create a CFD simulation that is solvable with normal PC performance and within a reasonable time, the number of elements has to be smaller than a few million. The representation of small clearances between screws and the liner can be done using many unstructured elements, but also with a limited number of well positioned elements, see chapter 3. Therefore, structured elements are preferred to unstructured elements.
In this chapter a method to divide a twin screw pump in structured hexahedral cells is discussed. This method consists of the layering of two-dimensional cross-sections, perpendicular to the axial direction, to form a three-dimensional grid. In section 4.1 quadrilateral cells will be placed on this cross-section, and in section 4.2 some refinements will be applied to this quadrilateral two-dimensional grid. In section 4.3 the quality of the two-dimensional and three-dimensional grid will be evaluated. In section 4.4 grid quality improvement by placing the nodes on another cross-section is evaluated. In section 4.5 conclusions about the applicability of the grid are discussed.

4.1 Basic structure

The algorithm described here, positions the nodes based on the solution of the Laplace equation in a two-dimensional section of the flow domain (see figure 4.1). The Laplace solution is obtained on an unstructured grid (figure 4.2(a)) of a cross-section normal to the axial direction with well-chosen boundary conditions. At this stage the boundary conditions for the potential Φ are: $\Phi = 0$ for the liner, $\Phi = -1$ for the left screw, and $\Phi = 1$ for the right screw. After solving this problem, equipotential values of this problem are given in figure 4.2(b). A valuable characteristic of the solution of the Laplace equation is that the equipotential lines never cross. Furthermore, the direction of the gradient $\nabla\Phi$ is perpendicular to the potential lines. With the present boundary conditions these gradient lines are also perpendicular to the boundaries. A grid based on equipotential and gradient lines can obtain high quality almost everywhere, except near the bottom and top cusp. Highly distorted cells are generated near the cusps since the potential line $\Phi = 0$ does not end in the top and bottom cusp. This is corrected with small adjustments in section 4.2. To expand this two-dimensional grid to three dimensions, two-dimensional grids with small axial distance apart are computed as described above. These two-dimensional grids have an equal number of radial and tangential nodes.

Now nodes with equal index are connected to form a three-dimensional mesh of hexahedral cells.
The position of the grid nodes are calculated with the CFD-program Comsol with MATLAB interface. The nodes are written in a mesh file suited for calculation with Fluent. Faces are grouped in inlet, outlet, screw and liner. In [9] and [10] methods to create a structured mesh are described. More detailed information of the screw is given in appendix B. Furthermore a theoretical screw profile without clearance is described in appendix A, to gain more insight in the shape of the screw. In table 4.1 the characteristic dimensions of the screw are given.

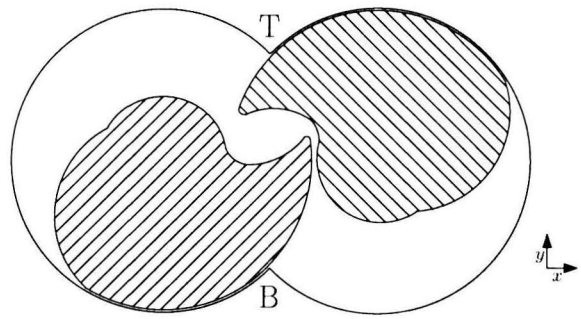

Figure 4.1: Cross-section of a twin screw pump, indicating top (T) and bottom (B) cusps (not to scale)

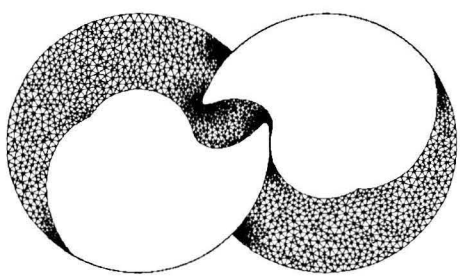

(a) Unstructured mesh of cross-section of a twin screw pump

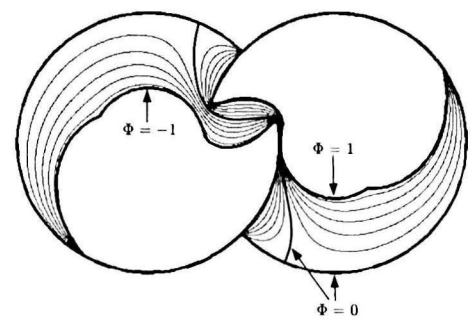

(b) Contourlines of potential value, with boundary conditions constant along each separate wall

Figure 4.2: Unstructured mesh and potential flow solution of cross-section of twin screw pump

4.2 Refinements

4.2.1 Dividing line

The equipotential line $\Phi = 0$ does not give a satisfactory dividing line between the left and right screw. A smooth dividing line from top to bottom cusp is created by: firstly changing the boundary conditions, and secondly, defining a line with a potential dependent on the vertical coordinate y. The boundary condition on the liner becomes a linearly changing potential

Table 4.1: Dimensions of twin screw pump

Screw outer radius	R	147.25 mm
Screw inner radius	r_i	62.5 mm
Liner radius	R_{liner}	147.5 mm
Center offset	h	210 mm
Clearance screw - liner	s	$0.24 - 0.265$ mm
Clearance screw - screw		$0.29 - 0.38$ mm
Pitch of the screw	r	60 mm
Number of threads	n_{rev}	$5\frac{1}{3}$
Radius rounded edges		0.5 mm

from Φ_T to Φ_B. The boundary conditions of the screws remain the same. The values of Φ_T and Φ_B are chosen iteratively so that the line with constant potential (Φ_T or Φ_B) departing from the cusp edge lies between the two tangents of the liner, represented by the dashed line in figure 4.3(a). The dividing line with a varying potential Φ_D, so that a smooth line from top to bottom cusp arises (see figure 4.3(b)), is defined as:

$$\begin{aligned} y \leq \alpha \quad \Phi_D &= \Phi_B \cdot \left(\frac{1 + \cos(\frac{y \cdot \pi}{\alpha})}{2} \right)^{\beta} \\ \alpha < y \leq 1 - \alpha \quad \Phi_D &= 0 \\ y > 1 - \alpha \quad \Phi_D &= \Phi_T \cdot \left(\frac{1 + \cos(\frac{(1-y) \cdot \pi}{\alpha})}{2} \right)^{\beta} \end{aligned} \tag{4.1}$$

where y is the normalized vertical distance, see figure 4.1. The parameter y changes from zero in cusp B to one in cusp T. The constants α and β are chosen to create a smooth dividing line, here $\alpha = 0.345$ and $\beta = 0.67$ are chosen.

4.2.2 Smoothing of nodes on gridline starting on the cusps

The radial gridlines starting on the cusps have an equidistant node placement, and this results in non-orthogonal cells (see figure 4.4(a)). It suffices to move these nodes to a spline created from neighboring cells on the same tangential line. This movement gives a grid near the top cusp as given in figure 4.4(b).

4.2.3 Non-equidistant node placement

On the liner and the dividing line, nodes are placed equidistantly. From these nodes, gridlines towards the screws emerge, which are directed along the potential gradients. These gridlines are then partitioned equidistantly to obtain the nodes of the structured two-dimensional grid. Since the potential does not have a constant value on the liner and the dividing line, the resulting gridlines are not orthogonal to the wall, nor are the grid cells orthogonal themselves. However the deviation turns out to be small in practice.

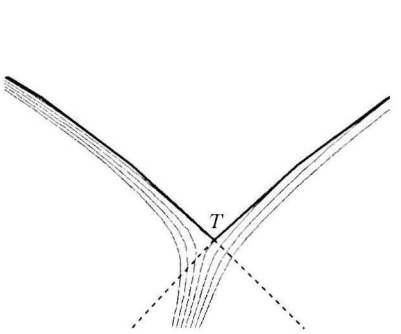

(a) Potential lines near the top cusp in a cross-section of a twin screw pump

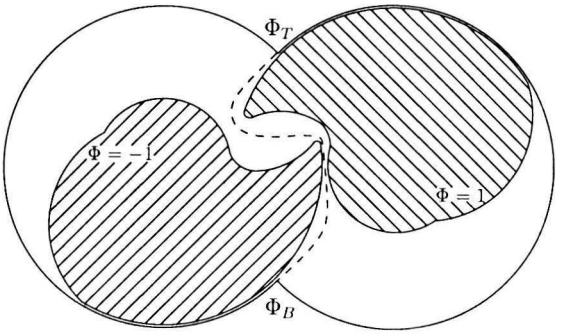

(b) Dividing line between top and bottom cusps, with linear varying boundary condition on the liner from Φ_T to Φ_B (not to scale)

Figure 4.3: Radial line near cusp

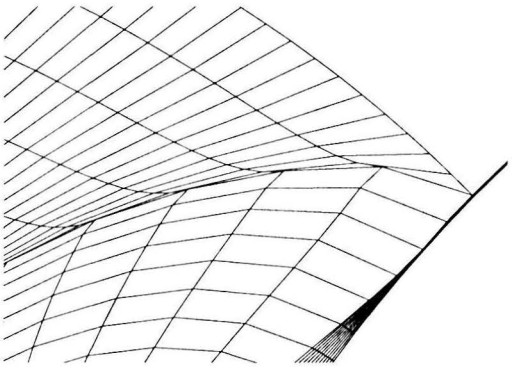

(a) No adjustment of radial gridline starting in cusp

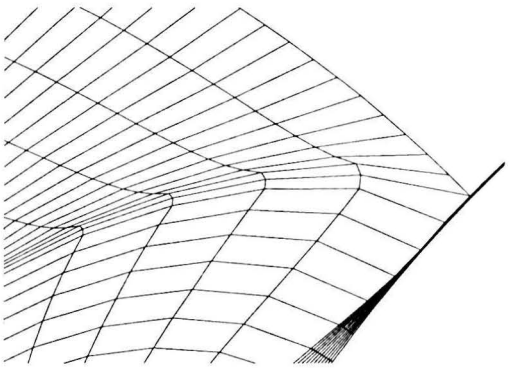

(b) Adjusted radial gridline starting in cusp

Figure 4.4: Gridlines near the top cusp in a cross-section of a twin screw pump

Gridlines, starting at points on the dividing line, towards the left and right screw have different lengths. With equidistant placement of the nodes, a discontinuity in cell volume exists. A refinement to the equidistant placing of the nodes is applied. The longest gradient line is divided in elements with a linear grow rate q, see figure 4.5. To avoid a discontinuity in cell volume for cells at the transition of dividing line and liner, nodes on gridlines starting at points on the liner are also placed non-equidistant.
In figure 4.6 the two-dimensional grid for a cross-section is given. The discontinuity in the area of the cells, near the dividing line, is clearly visible with equidistant node placement. Non-equidistant node placement reduces this discontinuity significantly. The linear grow rate q is limited, this to prevent the formation of extremely large cells at the screw surface and discontinuities in cell volume in other parts of the domain than near the dividing line. With non-equidistant node placement, a three-dimensional grid of the twin screw pump is generated, the surface mesh of the screws is displayed in figure 4.7.

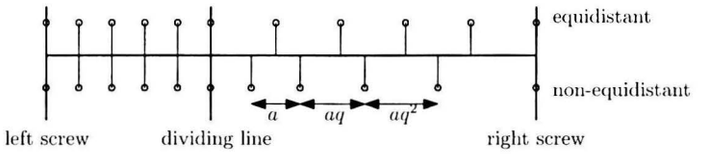

Figure 4.5: Equidistant and non-equidistant node placing

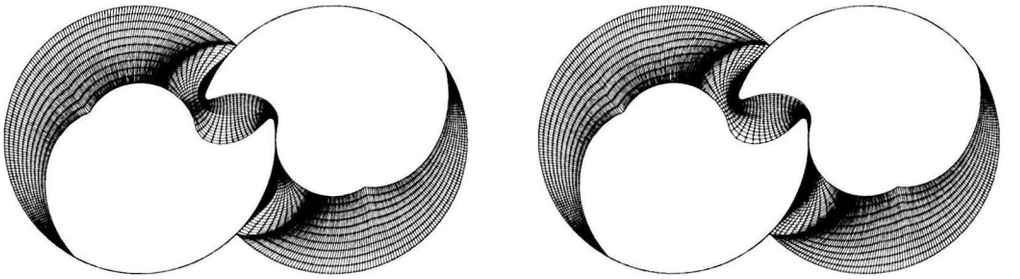

(a) Equidistant node placement (b) Non-equidistant node placement

Figure 4.6: Refined quadrilateral grid of a cross-section of a twin screw pump

4.3 Grid evaluation

The two-dimensional and the three-dimensional grid will be evaluated on skewness, and the three-dimensional grid also on volume ratio of neighboring cells. First the theory of the two methods is discussed in section 4.3.1 and applied in section 4.3.2.

4.3.1 Theory

A normalized measure of skewness is EquiAngle Skew (Q_{EAS}), which is defined for an individual grid cell as:

$$Q_{EAS} = \max\left\{\frac{\theta_{\max} - \theta_{eq}}{180 - \theta_{eq}}, \frac{\theta_{eq} - \theta_{\min}}{\theta_{eq}}\right\} \tag{4.2}$$

where $\theta_{\max}$ and $\theta_{\min}$ are the maximum and minimum angles (in degrees) between the edges of the cell, and θ_{eq} is the characteristic angle corresponding to an equilateral cell of similar form. For triangular and tetrahedral cells, $\theta_{eq} = 60$. For quadrilateral and hexahedral cells, $\theta_{eq} = 90$. It can be applied to two-dimensional as well as three-dimensional grids.
By definition,

$$0 \leq Q_{EAS} \leq 1 \tag{4.3}$$

where $Q_{EAS} = 0$ describes an equilateral cell, and $Q_{EAS} = 1$ a degenerated cell. Table 4.2 outlines the overall relationship between Q_{EAS} and cell quality.

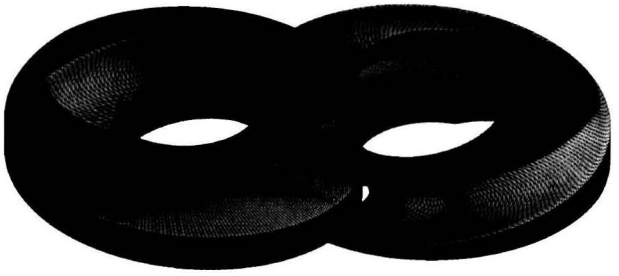

Figure 4.7: Three-dimensional structured screw surface mesh for one thread of a twin screw pump (color indicating axial coordinate)

Table 4.2: Q_{EAS} vs. Mesh Quality

Q_{EAS}	Quality
$Q_{EAS} = 0$	Equilateral (Perfect)
$0 < Q_{EAS} \leq 0.25$	Excellent
$0.25 < Q_{EAS} \leq 0.5$	Good
$0.5 < Q_{EAS} \leq 0.75$	Fair
$0.75 < Q_{EAS} \leq 0.9$	Poor
$0.9 < Q_{EAS} \leq 1.0$	Very Poor
$Q_{EAS} = 1$	Degenerate

In general, high-quality meshes have an average Q_{EAS} value of 0.1 for two-dimensional grids, and 0.4 for three-dimensional grids.

Volume ratio VR only applies to three-dimensional cells. A common method to calculate the volume of hexahedral cells in numerical simulations is to estimate the volume of a tetrakis hexahedron. The volume of a tetrakis hexahedron is given by equation (4.4). A tetrakis hexahedron are 24 tetrahedrals that form a hexahedral. The numbering of the nodes is given in figure 4.8. For derivation of this equation reference is made to [3].

$$\begin{aligned} V = & \frac{1}{12}\det\left[(\vec{x}_7 - \vec{x}_1) + (\vec{x}_6 - \vec{x}_0), (\vec{x}_7 - \vec{x}_2), (\vec{x}_3 - \vec{x}_0)\right] + \\ & \frac{1}{12}\det\left[(\vec{x}_6 - \vec{x}_0), (\vec{x}_7 - \vec{x}_2) + (\vec{x}_5 - \vec{x}_0), (\vec{x}_7 - \vec{x}_4)\right] + \\ & \frac{1}{12}\det\left[(\vec{x}_7 - \vec{x}_1), (\vec{x}_5 - \vec{x}_0), (\vec{x}_7 - \vec{x}_4) + (\vec{x}_3 - \vec{x}_0)\right] \end{aligned} \tag{4.4}$$

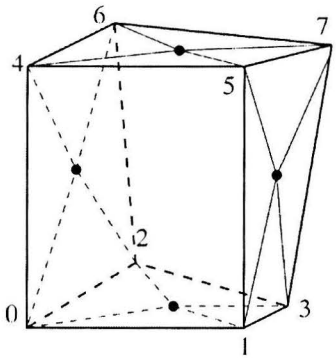

Figure 4.8: Tetrakis hexahedron with face-centered vertices (subdivision of front and back faces not drawn)

The volume ratio VR is defined as the maximum ratio of the volume of an cell with the volume of adjacent cells normalized between 0 and 1, according to:

$$VR = \min_i \left(\min \left(\frac{V_i}{V}, \frac{V}{V_i} \right) \right) \tag{4.5}$$

where i are the neighboring cells. A volume ratio of 1 represents cells with equal volume.

4.3.2 Evaluation

In figure 4.9 the values for Q_{EAS} are given for a two-dimensional grid of a cross-section and for one slice of three-dimensional cells. Mean value for the skewness in the two-dimensional and three-dimensional grids is 0.12 and 0.43 respectively. These mean values for Q_{EAS} normally represent a good quality grid, but from the distributions of Q_{EAS} (figure 4.9(d)) it is clearly visible that there are a large number of highly skewed cells in the three-dimensional grid. So, the grid is not as good as the average value of Q_{EAS} wants us to believe. Highly skewed cells in the two-dimensional grid are on radial lines starting near the cusps. Further refinements of the two-dimensional meshing method can improve the mesh. Near the flanges of the screw also highly skewed cells are created in the three-dimensional mesh. The skewness near the flanges cannot be improved by changing the grid of a cross-section. The number of skewed cells near the flanges is much larger than near the cusp, so no further refinements are made to the two-dimensional grid of a cross-section. The effect of elongation in axial direction on the skewness of the three-dimensional grid is evaluated. Elongation of the screw pump in axial direction improves the cell skewness. In table 4.3 the mean skewness Q_{EAS} for elongated structured three-dimensional grids of a twin screw pump is given. In figure 5.2 the skewness for a 2.5 and a 5 times elongated grid is given. The overall skewness improves, however some highly skewed cells remain present near the highly curved part of the screw (red area in figure 4.9(d)).
The volume ratio VR is low at the dividing line near the cusps of the twin screw pump, see figure 4.11. Changing the two-dimensional grid of a cross-section can improve the volume ratio. The grow rate q of cells on radial lines (section 4.2.3) is limited to ensure a high volume ratio in most part of the mesh, but is responsible for this discontinuity in volume at the dividing line.

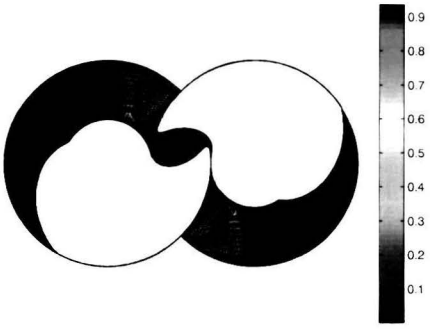

(a) Skewness of two-dimensional grid of a cross-section

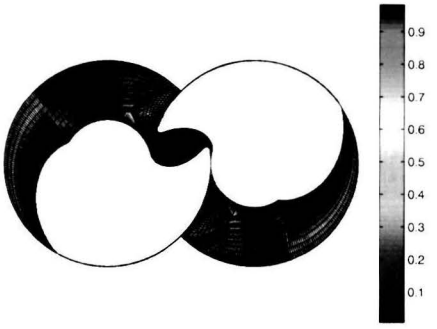

(b) Skewness of one layer of three-dimensional cells projected on cross-section

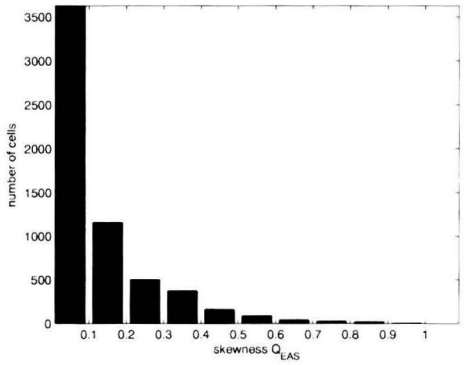

(c) Distribution of skewness for the two-dimensional grid of a cross-section

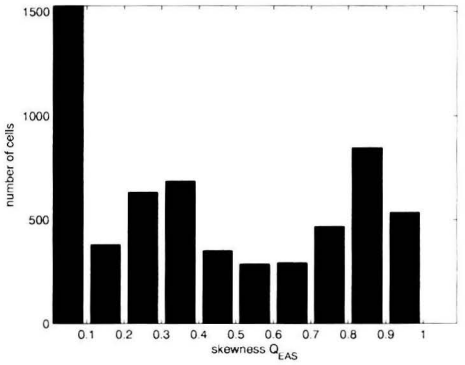

(d) Distribution of skewness for one layer of three-dimensional cells

Figure 4.9: Skewness Q_{EAS}

4.4 Three-dimensional basis structure

The quality of the two-dimensional grid is not the limiting factor. The expansion to three dimensions gives skewed cells. This favours the idea of solving the potential problem in three dimensions, and using the equipotential surfaces and gradient lines as a basis for a three-dimensional grid. Gradient lines depart perpendicular to the wall, so grid skewness should be improved. To solve the three-dimensional potential problem, first a three-dimensional grid of the screw is needed. A potential problem is known to pose less stringent demands to the grid quality. Therefore, the skewed three-dimensional structured grid can be used. Secondly, the improvement of the grid has to be evaluated. To determine the quality of the grid, a cross-section in axial direction of the twin screw pump is made and the potential problem is solved in two dimensions with the following boundary conditions: liner $\Phi = 0$ and screw $\Phi = 1$. In figure 4.12(a) gradient lines are drawn. These lines are not ideal, since many lines accumulate in the center of the cavity. By changing the boundary conditions this can be prevented. Dividing the gradient lines equidistantly gives quadrilateral cells, see figure 4.12(b). In figure 4.12(c) the distribution of skewness Q_{EAS} is given for this grid. The skewness for this two-

Table 4.3: Mean skewness Q_{EAS} for elongated grids in axial direction

Elongation e	mean skewness Q_{EAS}
1	0.43
2	0.35
2.5	0.33
5	0.26
10	0.21

dimensional section in axial direction is similar to the three-dimensional structured grid of the twin screw pump already described. Placing nodes on basis of the three-dimensional potential problem therefore does not improve the quality of the mesh much, and is not employed.

4.5 Conclusion

A method to describe a twin screw pump with structured hexahedral cells is developed. Two-dimensional structured grids of cross-sections perpendicular to the axial direction are layered to a structured three-dimensional grid. The two-dimensional grid on a cross-section is placed along gradient lines of the Laplace problem. The Laplace problem is solved on an unstructured grid of the cross-section with suitable Dirichlet boundary conditions. Some adjustments are made to improve the quality of the two-dimensional grid. All two-dimensional grids have the same topology, this is required to combine all two-dimensional grids to a three-dimensional grid. The quality of the three-dimensional grid, in terms of skewness, deteriorates due to the high surface curvature of the geometry, compared to the quality of the two-dimensional grid. Placing the gridlines along the equipotential surfaces and gradient lines of a three-dimensional Laplace problem gives a skewness similar to the three-dimensional grid created with the layering method, so this is no improvement of the grid.

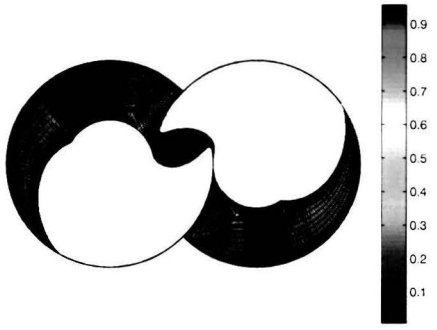

(a) Skewness for one layer of three-dimensional cells of a 2.5 times elongated grid in axial direction

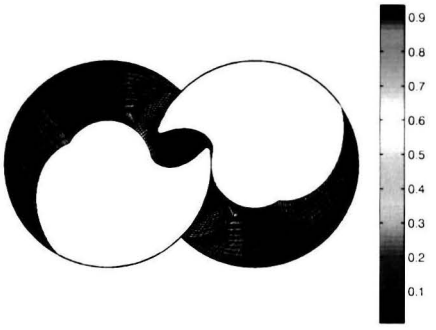

(b) Skewness for one layer of three-dimensional cells of a 5 times elongated grid in axial direction

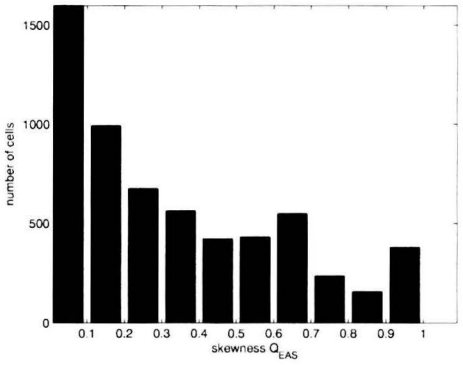

(c) Distribution of skewness for one layer of three-dimensional cells of a 2.5 times elongated grid in axial direction

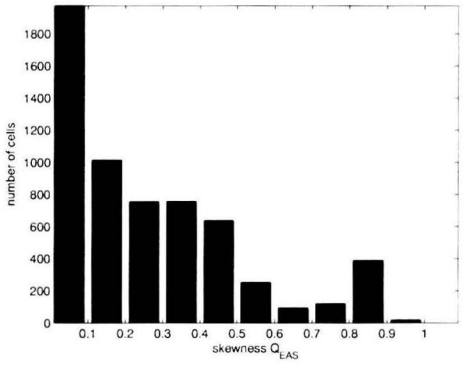

(d) Distribution of skewness for one layer of three-dimensional cells of a 5 times elongated grid in axial direction

Figure 4.10: Skewness Q_{EAS} of an elongated twin screw pump in axial direction

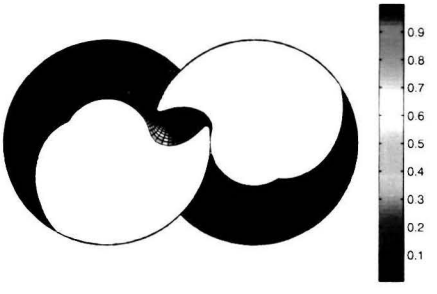

(a) Volume ratio VR of one layer projected on cross-section

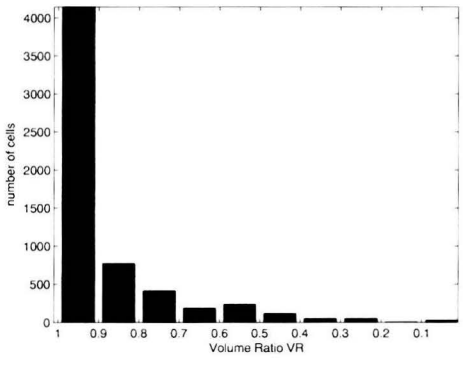

(b) Distribution of volume ratio

Figure 4.11: Volume ratio VR

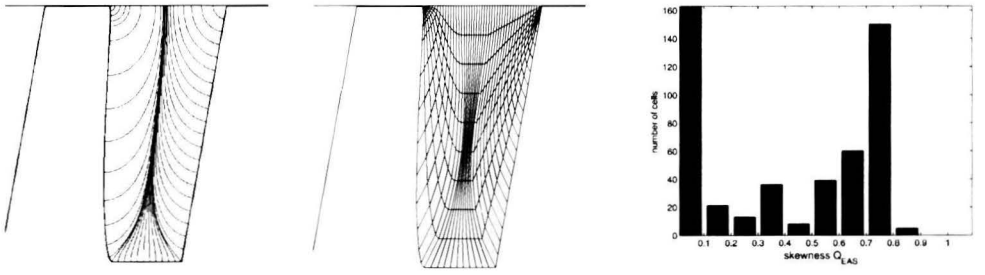

(a) Gradient lines of Laplace problem with boundary conditions constant along each wall

(b) Structured quadrilateral grid for an axial cross-section of a screw

(c) Distribution of skewness for an axial cross-section of a screw

Figure 4.12: Cross-section in axial direction of one screw thread

Chapter 5

CFD computations with structured grid

5.1 Numerical set-up

With the structured grid generated in chapter 4, three-dimensional flow calculations are performed. The grid consists of one screw thread of the twin screw pump and each screw has 10 radial cells, 300 tangential cells, and 180 axial cells (see figure 4.7). Thus the total number of hexahedral cells is approximately 1 million. The leakage flow rate through periodic stationary screws is calculated for a fixed pressure drop over the screw thread. The flow is simulated with the steady segregated solver and implicit formulation, turbulence is modeled with the standard $k-\omega$ model with standard wall function. For the initial condition the velocity and the turbulent kinetic energy are set to zero in the complete domain, and the specific dissipation rate of the turbulence to one. Water is taken as the leakage medium. Also calculations on an elongated twin screw pump are performed to evaluate the effect of screw geometrie and skewness of the grid.

5.2 Results

There are three cases tested. First, the leakage flow through a twin screw pump is simulated at low axial Reynolds numbers. The axial Reynolds number varies from 19 to 381 in the clearances between screw and liner. Secondly, the leakage flow is simulated for an elongated twin screw pump in axial direction at approximately equal Reynolds number in the clearance between screw and liner. Thirdly, for a 5 times elongated grid of a twin screw pump the leakage flow is simulated for axial Reynolds numbers up to 1514.
The total leakage flow rate is compared with the leakage flow rate through the clearances between screw and liner. In figure 5.1(a) the clearance between the screw and liner is given by region 2. Also the mean axial velocity through the clearance between screw and liner is compared with the analytical equation for laminar flow in an annulus with and without inlet and outlet resistances, given in equation (2.4).
The low quality of the grid results in non converging solutions with the standard parameters. By lowering the under-relaxation factors and taking a low differential pressure per screw thread, a converged leakage flow rate is calculated. A under-relaxation factor reduces the change of the variable for the next iteration.

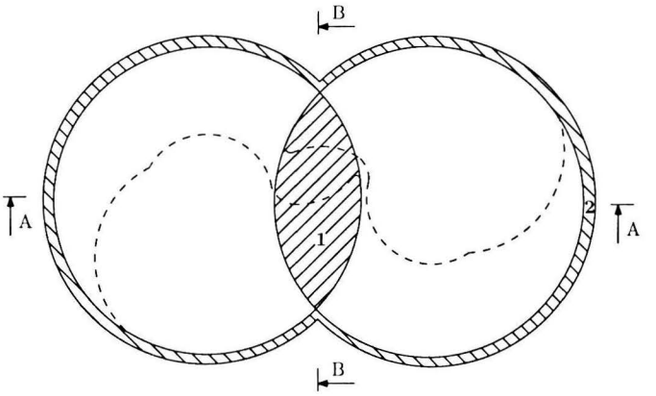

(a) Regions of leakage: 1 between screws and 2 between screw and liner. Cross-section A-A given in figure 5.2(a) (not to scale)

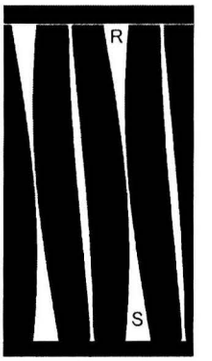

(b) Cross-section B-B

Figure 5.1: Cross-sections of twin screw pump

In the first case of the three-dimensional flow simulations the pressure drop is set from 300 to 9600 Pa over one screw thread. For water the differential pressure should be approximately 130 kPa over one screw thread for realistic flow and a axial Reynolds number of 2230. At a higher differential pressure than 9600 Pa over one screw thread the solution is non-converging, even with low under-relaxation factors. The used pressure difference per seal is low, resulting in a low axial leakage velocity, and a low dimensionless wall distance. The effect of the dimensionless wall distance on the turbulence model is discussed in chapter 2 and should be greater that 11 for wall functions. The dimensionless wall distance in the clearance is lower than the required value, it varies from 0.5 to 3 for the different axial Reynolds numbers. No accurate solution of the numerical simulation can be expected, but some tendencies are visible. In table 5.1 the simulated leakage flow rate for a stationary twin screw pump is given for different differential pressures over the screw. The leakage percentage of fluid through the clearance between the screw and the liner compared to the total leakage flow rate $\dot{m}_2/\dot{m}$, is higher at a higher differential pressures over the screw. The simulated mean axial velocity in the clearance between screw and liner is compared to the flow rate in an annulus from equation (2.4) with and without in- and outlet resistances. For a non-rotating stationary annulus, the resistance coefficient is $\lambda = 48Re^{-1}$ [11] for laminar flow.

In the second case the grid is elongated, the elongation of the grid changes the dimensions of the two leakage regions (figure 5.1(a)). First region 1, the clearance between the screws gets larger and the flow resistance reduces. Elongation in axial direction reduces the flow resistance from region R to S in figure 5.1(b). Secondly region 2, the length of the clearance between screw and liner gets larger and thus becomes a larger flow resistance. Elongation in axial direction increases the length of the clearance between region O and P in figure 5.2(a). In table 5.2 the leakage flow rate is given for elongated screws with a laminar leakage flow rate in the clearances between screw and liner.

In the third case a 5 times elongated grid in axial direction is used and the differential pressure over the screw is varied. The axial Reynolds number in the clearance between

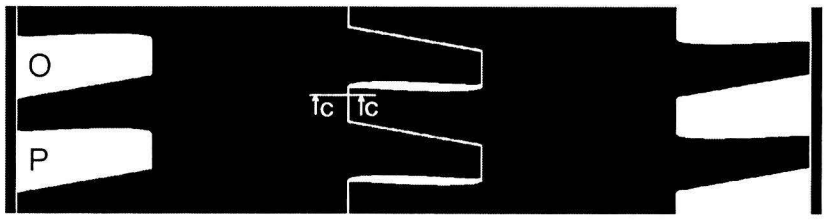

(a) Cross-section A-A in axial direction of two threads (black: screw/liner, white: fluid)

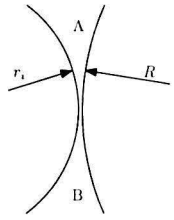

(b) Cross-section C-C (not to scale)

Figure 5.2: Cross-sections of twin screw pump

screw and liner varies from 20 to 1500. There is no converged solution found for higher axial Reynolds numbers. In table 5.3 the simulated leakage flow rate through the twin screw pump is given. The mean axial velocity in the clearance $\langle v_{ax} \rangle$ is given for the simulation and calculated with equation (2.4), with a value of 1.5 for in- and outlet resistance δ_{io}. In [11], the resistance coefficient for a stationary annulus is given as: $\lambda = 48Re^{-1}$ for laminar flow, and $\lambda = 0.26Re^{-0.24}$ for turbulent flow. The mean axial velocity of the numerical simulation and equation (2.4) are similar for laminar flow up to a Reynolds number of approximately 500. At higher axial Reynolds numbers, the simulated and calculated mean axial velocity deviate from each other. The dimensionless wall distance for an axial Reynolds number of 1514 on a 5 times elongated grid is given in figure 5.3. The value of the dimensionless wall distance y^+ in the clearance and in the cavity are approximately 8 and 1000 respectively.

Table 5.1: Water leakage flow rate for three-dimensional stationary twin screw pump simulations with various pressure differences per screw thread, $\langle v_{ax} \rangle$ in clearance between screw and liner

		$\langle v_{ax} \rangle$ $[m/s]$				
Δp $[Pa]$	$\dot{m}$ $[kg/s]$	eq. (2.4) $\delta_{io} = 0$	eq. (2.4) $\delta_{io} = 1.5$	numeric	Re	$\dot{m}_2$ / $\dot{m}$ [%]
300	0.7	0.072	0.072	0.074	19	4.0
600	0.9	0.144	0.142	0.145	37	5.7
1200	1.4	0.29	0.28	0.277	70	7.0
2400	2.1	0.58	0.54	0.51	129	8.6
4800	3.2	1.15	1.0	0.90	227	10.8
9600	4.8	2.3	1.8	1.51	381	11.1

5.3 Conclusion

The quality of the used grid is low, lowering under-relaxation factors only results in converged solutions for a low differential pressure over the twin screw pump. This low differential pressure results in a low leakage velocity and the dimensionless wall distance dependent on this velocity is too low to calculate an accurate solution with the $k - \omega$ turbulence model with wall functions. From the simulations some conclusions can be draw. First: elongation of the

Table 5.2: Water leakage flow rate for three-dimensional stationary twin screw pump simulations with 5000 Pa/m pressure difference for elongated grid in axial direction ($Re \approx 19$)

e	$\dot{m}$ $[kg/s]$	$\langle v_{ax} \rangle$ $[m/s]$	$\dot{m}_2$ / $\dot{m}$ [%]
1	0.7	0.0740	4.0
2	1.6	0.0762	1.7
2.5	2.1	0.0762	1.3
5	4.7	0.0745	0.6
10	8.0	0.0731	0.3

Table 5.3: Water leakage flow rate for three-dimensional stationary twin screw pump simulations for a 5 times elongated grid in axial direction, $\langle v_{ax} \rangle$ according to equation (2.4) with in- and outlet resistance for laminar and turbulent definition of λ

		$\langle v_{ax} \rangle$ $[m/s]$				
Δp $[kPa]$	$\dot{m}$ $[kg/s]$	laminar	turbulent	numeric	Re	$\dot{m}_2$ / $\dot{m}$ [%]
1.5	4.7	0.072	0.38	0.0745	19	0.6
3	6.6	0.14	0.57	0.15	38	0.8
6	9.4	0.29	0.84	0.29	73	1.1
12	12.9	0.57	1.2	0.57	144	1.6
24	18.3	1.1	1.8	1.08	273	2.1
48	26.2	2.2	2.7	1.9	482	2.6
96	37.6	4.1	4.0	2.9	740	2.8
192	52.4	7.3	5.8	4.0	1005	2.7
288	62.5	10.2	7.3	5.0	1262	2.8
384	75	12.7	8.6	6.0	1514	2.8

screws in axial direction results in a larger leakage flow for the same differential pressure over the screw thread. The leakage flow rate in the clearance between screw and liner reduces, however the leakage flow rate between the screws increases, even more than the decrease in the other region. Secondly: increasing the differential pressure per screw thread changes the leakage flow ratio between the two regions.
The leakage flow rate through the clearances between the screw and liner has a larger portion of the total leakage flow rate at a higher differential pressures for laminar flow. This can be expected from analytical equations. The relation between differential pressure and axial velocity is given in equation (2.4) for flow in an annulus. The differential pressure is approximately linearly proportional to the axial leakage velocity for laminar flow. For an expansion in the diameter of a pipe the relation between differential pressure and axial velocity is given in [8] and is $\Delta p = K \frac{1}{2} \rho v^2$, where K is a constant for turbulent flow. In the numerical simulations the value of K also remains approximately constant, even for laminar flow. In a twin screw pump the leakage flow between the screw and liner is similar to flow in an annulus, however the leakage flow between the screws is similar to a expansion in the diameter of a pipe. This expansion between the screws is most clearly visible in the cross-section given in

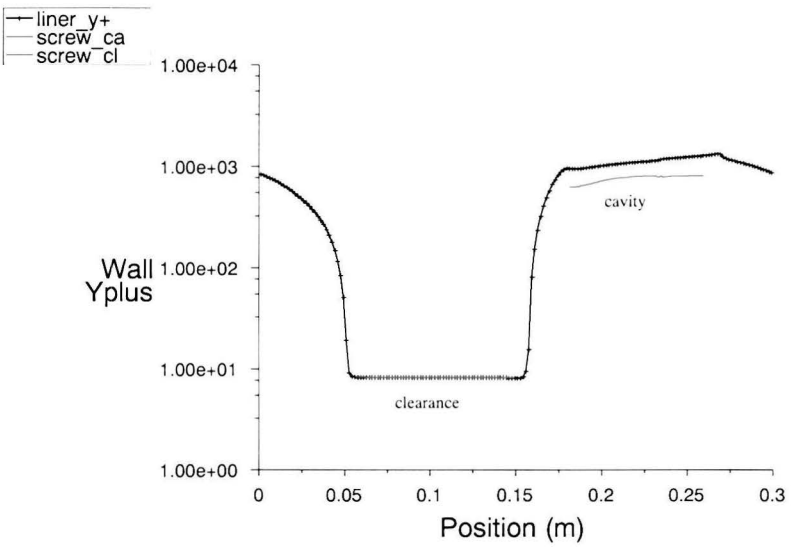

Figure 5.3: Dimensionless wall distance for $e = 5$ and pressure difference of 384 kPa over one thread for a twin screw pump (Re in the clearance is 1514)

figure 5.2(b) between region A and B, and also in figure 5.1(b) between region R and S.
At higher axial Reynolds numbers the ratio between leakage flow rate through the clearances and the total leakage flow rate is found constant in the numerical simulations. This indicates a constant resistance coefficient λ for axial Reynolds numbers above a certain number or a negligible effect of sealing length compared to in- and outlet resistances.

Chapter 6

Conclusions and recommendations

6.1 Final conclusion

To model the flow in a twin screw pump a grid of the screw pump has to be made. This grid has to describe the geometrie of the pump well. Also the turbulence model poses requirements on the dimensionless wall distance of the first cell at solid walls. To obtain a solution for the flow in a twin screw pump with normal PC performance and in reasonable time, the number of cells must be limited. A grid of the twin screw pump is made and the leakage flow through the twin screw pump is simulated for a low differential pressure over the pump.
The demands of the turbulence model are evaluated by comparison with the results of two experiments. First, the flow through an annulus with rotating inner cylinder is modeled. Near-wall modeling and wall functions are considered for the different variants of the $k-\epsilon$ and $k-\omega$ turbulence model. Secondly, the flow through a stationary straight-through labyrinth seal is simulated. Here only wall functions are considered for the different turbulence models. The standard $k-\omega$ model gives the most accurate results when simulating with wall functions. Wall functions are needed to keep the total number of cells limited. The dimensionless wall distance y^+ has to be larger than 11 to give accurate results with wall functions.
A mesh method is constructed that generates a structured hexahedral grid by layering of cross-sections perpendicular to the axial direction. The quality of the two-dimensional grid of a cross-section is good, however the three-dimensional grid has poor quality. The three-dimensional cells have a high skewness in some regions.

Between the screw and the liner structured cells with elongated sides in axial and tangential direction have to be used to keep the total number of cells limited. Numerical simulations proved that this elongation has no influence on the flow through an annulus with inner rotating cylinder. Gradients of the solution in axial and tangential direction are low compared to the radial direction.
From the simulations some conclusions can be drawn. First: elongation of the screws in axial direction results in a large leakage flow for the same differential pressure per screw thread. The leakage flow rate in the clearance between screw and liner reduces, however the leakage flow rate between the screws increases, even more than the decrease in the other region. Secondly: increasing the differential pressure per screw thread changes the leakage flow ratio between the two regions for the laminar flow regime. The leakage flow rate through the clearances between the screw and liner has a larger portion of the total leakage flow rate

at higher differential pressures. Besides the numerical result this is also expected from the analytical equations for the relation between differential pressure and axial fluid velocity in the two regions. At higher axial Reynolds numbers the leakage flow ratio between the two regions is approximately constant.

The static twin screw pump simulation shows realistic flow features at a low differential pressure over the pump. Expanding the simulation to a differential pressure present in industrial screw pumps gives a better understanding of the flow in a twin screw pump. The static simulations can be extended to a dynamic simulation with multiphase flow to obtain a complete model of the twin screw pump.

6.2 Recommendations

- The constructed three-dimensional grid has highly skewed cells, the grid quality has to be improved to allow accurate CFD simulations. On the existing grid small improvements can be made but it remains questionable if the quality will improve enough to perform accurate CFD simulations. There is another method of meshing the twin screw pump, while fulfilling the demands set in this report. This method consists of a hybrid grid, meaning a mixed grid of hexahedral and tetrahedral cells. The clearance between the screw and liner can be meshed with a structured hexahedral mesh and the interior with unstructured tetrahedral cells. The nodes on the interface either have to coincide, or a non-conformal interface (section 3.3) can be used.

- For comparison of twin screw pump simulations with experiments, measurements of the flow in the twin screw pump are needed.

- There are some small improvements possible on the construction of the cross-sectional mesh. Like: automatic determination of Φ_T, Φ_B, correctly describe the round-off of the screw tips, and curvature dependent distribution of nodes at the dividing line. This mesh can be used, for example, for a twin screw pump with a larger screw pitch.

- The multiphase modeling packages in Fluent should be tested on validation cases, to determine which model is the most accurate for flow in a twin screw pump.

- To create a time-dependent simulation, use can be made of smoothing and remeshing in Fluent. Smoothing and remeshing can deteriorate the mesh. When the mesh deteriorates beyond a certain limit, a new mesh can be used and the old solution can be interpolated on the new grid. This method has proven its applicability on a completely unstructured mesh of one screw thread of a twin screw pump with large clearances of 6 mm at consulting company Bunova Development BV.

- Validate behaviour of turbulence models for laminar flow in the clearance between screw and liner. There is laminar flow present when more viscous oil is pumped. A turbulence model is needed because in a dynamic simulation there are regions with turbulent flow.

- The first cells near the wall in a cavity are too large, resulting in a high dimensionless wall distance. So, adjustment of the grid in the cavities is necessary.

Bibliography

[1] Karassik et al. *Pump handbook*, pages 3.99–3.121. Mc Graw-Hill, third edition, 2001.

[2] W. Matek et al. *Roloff/Matek Machineonderdelen.* Academic service, third edition, 2000.

[3] J. Grandy. Efficient computation of volume of hexahedral cells. http://www.osti.gov/bridge/servlets/purl/632793-4p2OLa/webviewable/ Report number: UCRL-ID-128886.

[4] Fluent Inc. Fluent 6.2 user's guide.

[5] B.V.S.S.S. Prasad and V. Sethu Manavalan. Computational and experimental investigations of straight - through labyrinth seals. *"ASME Paper 97-GT-326"*, 1997.

[6] J.J.M. Smits. Modeling of a fluid flow in an internal combustion engine. Graduation report TU/e, Report number WVT 2006.22.

[7] A. Uasghiri. Een multigrid versnelling van de simple methode voor incompressible stromingen. Graduation report TU Delft (http://ta.twi.tudelft.nl/nw/users/vuik/numanal/uasghiri.html).

[8] Bart van Esch and Erik van Kemenade. Procestechnische constructies 1 - 4b660. Lecture notes, March 2005.

[9] J. Vande Voorde and J. Vierendeels. ALE calculations of flow through rotary positive displacement machines. *"Proceedings of FEDSM2005"*, (FEDSM2005-77353), 2005.

[10] J. Vande Voorde, J. Vierendeels, and E. Dick. Development of a laplacian-based mesh generator for ALE-calculations in rotary voluemtric pumps and compressors. *"J. Comput. Methods Appl. Mech. Engrg."*, (193):4401–4415, 2004.

[11] Y. Yamada. Resistance of flow through an annulus with an inner rotating cylinder. *"Bull. JSME"*, 5(1):302–310, 1962.

Appendix A

Theoretical Screw profile

The screw profile is described with a cross-section normal to the axial direction of the twin screw pump, see figure A.1. In this figure profile A and B are visible.

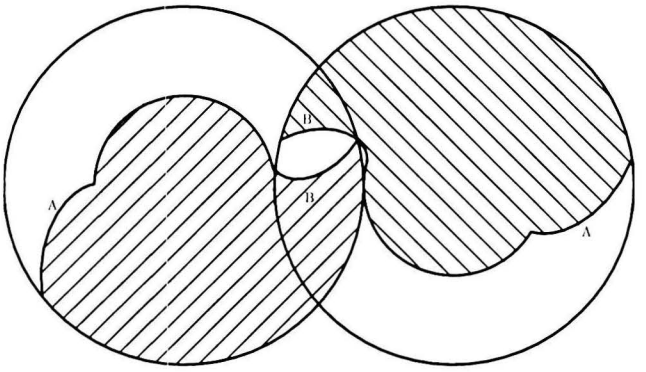

Figure A.1: Cross-section twin screw pump

The profile A is an involute profile (x and y) and described by the following equations:

$$s = \alpha r \tag{A.1}$$
$$x_c = r\cos\alpha \tag{A.2}$$
$$y_c = r\sin\alpha \tag{A.3}$$
$$x = x_c + s\sin\alpha \tag{A.4}$$
$$y = y_c - s\cos\alpha \tag{A.5}$$

where $r \leq r_i$, with r_i, the screw inner diameter. x_c and y_c are construction points on the circle with radius r. In figure A.1, r is equal to r_i. The other variables of profile A are defined in Figure A.2.
The profile B is described in polar coordinates θ and R by equations (A.6:A.10). The variables of profile B are defined in Figure A.3.

$$a = r_o\cos\alpha \tag{A.6}$$

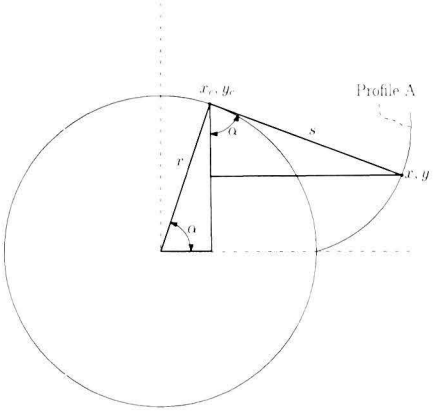

Figure A.2: Variables for profile A

$$h = r_o \sin\alpha \tag{A.7}$$
$$b = y - a \tag{A.8}$$
$$R = \sqrt{b^2 + h^2} \tag{A.9}$$
$$\theta = \pi + \alpha + \tan^{-1}(h/b) \tag{A.10}$$

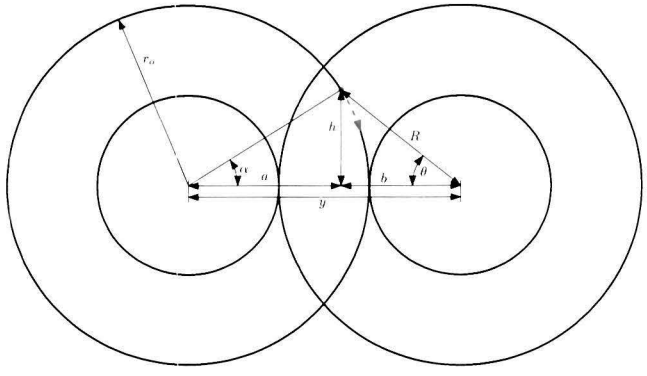

Figure A.3: Variables for profile B

Appendix B

Screw profile Houttuin

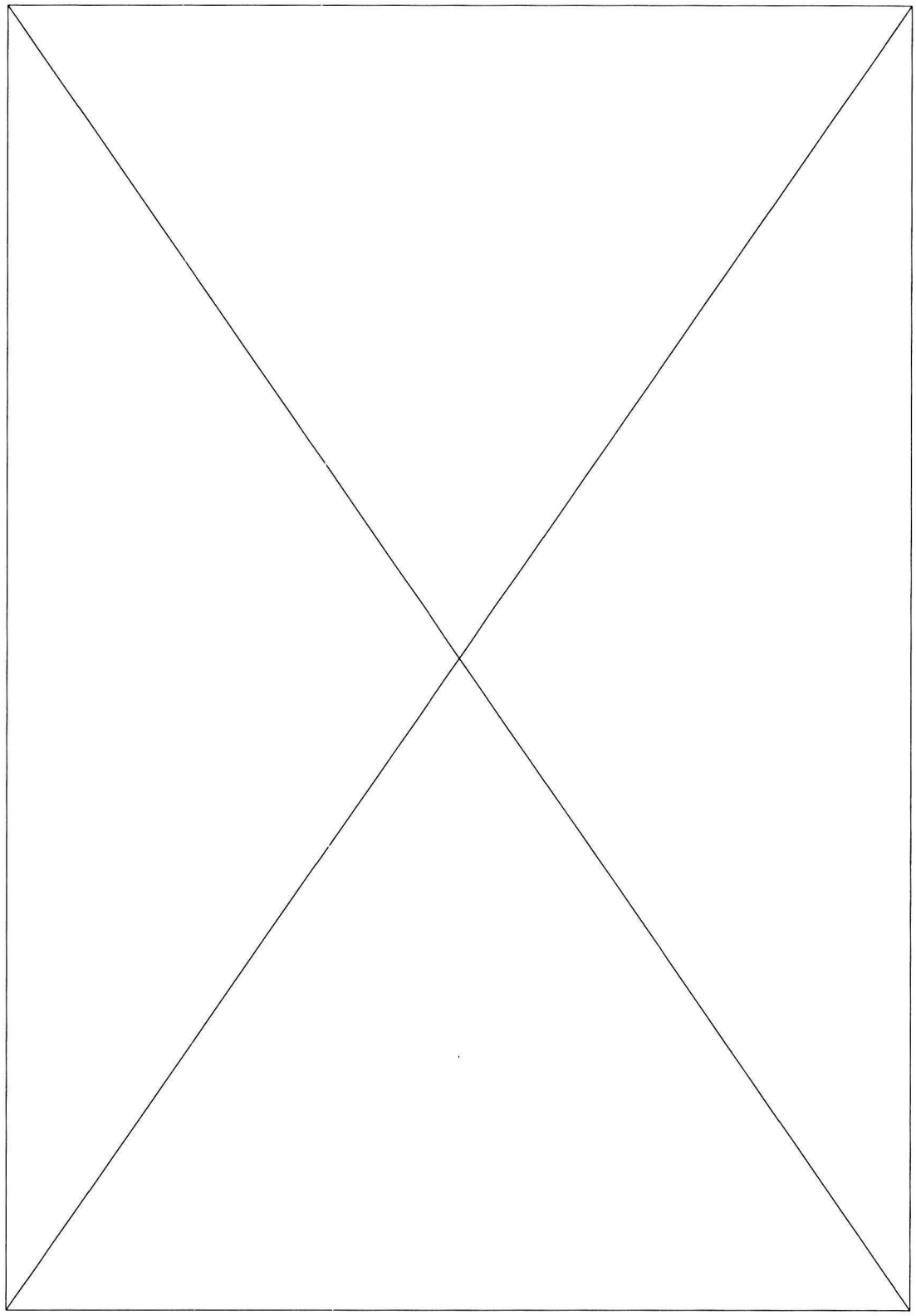

Acknowledgements

First of all I would like to thank my supervisor Bart van Esch for his help and guidance in completing my graduation project. Furthermore I like to thank the consulting company Bunova Development BV in Zwolle for creating this graduation report. Especially I would like to thank Timco Visser and Joàn Teerling for answering practical questions regarding the numerical model. Finally I would like to thank my roommates and my colleague graduate students for the pleasant and stimulating working atmosphere.

Maarten van Beijnum